Apical tuft input efficacy in layer 5 pyramidal cells from rat visual cortex

Paul A. Rhodes and Rodolfo R. Llinás

Department of Physiology and Neuroscience, New York University Medical School, 550 1st Avenue, New York, NY 10016, USA

(Resubmitted 11 December 2000; accepted after revision 12 April 2001)

1. The integration of synaptic inputs to the apical dendrite of layer 5 neocortical pyramidal cells was studied using compartment model simulations. The goal was to characterize the generation of regenerative responses to synaptic inputs under two conditions: (a) where there was an absence of background synaptic input, and (b) when the entire cell surface was subjected to a uniform blanket of synaptic background conductance such that somatic input resistance was reduced 5-fold.

2. Dendritic morphology corresponded to a layer 5 thick-trunked pyramidal cell from rat primary visual cortex at postnatal day 28 (P28), with distribution of dendritic active currents guided by the electrophysiological characteristics of the apical trunk reported in this cell type. Response characteristics for two dendritic channel distributions were compared, one of which supported Ca^{2+} spikes in the apical dendrite.

3. In the absence of background, synaptic input to the apical tuft was surprisingly effective in eliciting somatic firing when compared with input to apical oblique branches. This result obtained even when the tuft membrane was the least excitable in the dendritic tree.

4. The special efficacy of tuft input arose because its electrotonic characteristics favour development of a sustained depolarization which charged the apex of the apical trunk to its firing threshold; once initiated in the distal trunk, firing propagated inward to the soma. This mechanism did not depend upon the presence of depolarizing channels in tuft membrane, but did require an excitable apical trunk.

5. Rather than disconnect the tuft, background synaptic conductance enhanced the efficacy advantage enjoyed by input arriving there. This counterintuitive result arose because background reduced the subthreshold spread of voltage, and so diminished the ability of the excitation of various individual oblique branches to combine to charge the relatively thick adjacent trunk. In contrast, drive from the depolarized tuft is exerted at a single critical point, the apex of the distal trunk, and so was relatively undiminished by the background. Further, once initiation at the apex occurred, background had little effect on inward propagation along the trunk.

6. We conclude that synaptic input to the apical tuft of layer 5 cells may be unexpectedly effective in triggering cell firing *in vivo*. The advantage in efficacy was not dependent upon the characteristics of tuft membrane excitability, but rather stemmed from the geometry of the tuft and its junction with the distal apical trunk. The efficacy of tuft input was, however, critically dependent upon inward propagation, suggesting that modulation of membrane currents which affect propagation in the apical trunk might sensitively control the efficacy of tuft input.

It is now widely recognized that dendritic membrane is electrically active, and a growing body of data characterize types and densities of voltage-gated ion channels in dendrites (e.g. Llinás, 1988; Johnston *et al.* 1996). What then are the consequences entailed for the integration of inputs in active dendritic trees (Spencer & Kandel, 1961; Llinás *et al.* 1968, 1975)? In particular, how does the efficacy of synaptic input depend upon its spatial location and temporal pattern? The efficacy of a given synaptic input can clearly be altered by the non-linear responses of active membrane currents distributed in the dendritic tree, and so intuition derived from passive cable theory may not be a reliable guide.

Input to the apical tuft, a branching of the distal apical dendrite of pyramidal cells, has been considered unlikely to be capable of firing the cell (e.g. Vogt, 1991) because in passive dendritic models the efficacy of this distal synaptic input, which may arrive 1000 μm from the somata of layer 5 pyramidal cells, is small (e.g. Stratford *et al.* 1989). However, studies in which inputs to the tuft have been isolated in slices (Cauller & Connors, 1992) have found that tuft input can fire the cell body. The potential of apical tuft inputs to fire the cell enables heretofore little-considered functional roles for the layer 1 axon fibre system, a primitive element of cortical architecture present in three-layer turtle dorsal cortex (Desan, 1984; Ulinski, 1990), hippocampal and piriform cortices, as well as mammalian six-layer neocortex.

To examine the efficacy of inputs to the apical tuft of layer 5 cortical pyramidal cells and compare it to that of more proximal apical input we employed compartment model simulations (Rall, 1964). Specification of the density of ionic conductances in the dendritic tree was guided by data reporting direct measurement in dendritic patches of the apical trunk (Huguenard *et al.* 1989; Stuart & Sakmann, 1994; Stuart *et al.* 1997; Bekkers, 2000*a*,*b*), and further constrained by the requirement that the characteristics of both simulated backpropagation and dendritic Ca^{2+} spikes were consistent with those reported in dendritic impalement experiments (Amitai *et al.* 1993; Kim & Connors, 1993; Schiller *et al.* 1997; Stuart *et al.* 1997; Larkum *et al.* 1999*a*,*b*).

Much of the available data on single neuron properties and on the efficacy of synaptic inputs have necessarily been collected in slices of cortex, in which spontaneous activity and hence synaptic input to the measured cells is low. In the active brain a much higher average level of both excitatory and inhibitory presynaptic transmitter release undoubtedly exists, and, as has been noted (e.g. Holmes & Woody, 1989), this synaptic background input will alter the integrative properties of the dendritic tree. To develop predictions applicable to the case where synaptic background is present, simulations were performed in two conditions: in one background input was absent while in the other the entire dendritic tree and soma were blanketed by a background of synaptic input adequate to reduce somatic input resistance 4- to 5-fold as recently reported *in vivo* (Destexhe & Paré, 1999). NMDA conductance was included in this background, and so its non-linear implications have been incorporated in the simulations.

The results suggest that input to the apical tuft may be among the most effective that layer 5 cells receive. This finding does not presume a high density of depolarizing ion channels in the tuft itself, but rather depends on the electrotonic properties of the apical tuft and the adjoining apex of the apical trunk, and on the excitability of membrane in the distal trunk where the decisive initiation occurs. Further, background conductance appears not to disconnect distant input as might have been expected, but rather enhances the comparative advantage of synaptic input to the tuft. This simulation prediction, if confirmed experimentally, argues for a re-evaluation of the importance of layer 1 input to the pyramidal cell apical tuft in triggering the firing of pyramidal cells *in vivo*.

Some of these findings have been presented previously in abstract form (Rhodes & Llinás, 1999).

METHODS

Morphology and electrotonic membrane properties of the model layer 5 cell

Dendritic tree morphology and spine densities, which were kindly provided by Dr G. Major (University of Oxford), were taken from a layer 5 thick trunked cell in the primary visual area of 4- to 6-week-old rat cortex. A 400 μm length of axon, broken into compartments (1 μm diameter) was appended to the soma, with no special hillock morphology. Membrane resistance, cytoplasmic resistivity, and membrane capacitance were set at 50 000 $\Omega\,cm^2$, 200 $\Omega\,cm$, and 1 $\mu F\,cm^{-2}$, respectively. Spine density per unit membrane area was constant, 2 spines per μm length per μm width (see also Larkman, 1991), with the exception of those segments in the proximal trunk and branch initial segments, which were aspinous. We accounted for the presence of spines by assuming they were passive and adding their membrane area to each compartment, following Holmes (1989). The membrane area used per spine was 1.4 μm^2 which would, for example, correspond to a spine with a spherical head of 0.6 μm diameter and a cylindrical neck 0.1 $\mu m \times 1.0\,\mu m$. Thus in those dendritic segments containing spines we multiplied membrane capacitance and divided membrane resistance by the factor 1.92. With the foregoing assumptions, input resistance (R_{in}) of the simulated cell, measured with a 0.05 nA current step applied with dendritic membrane channels in place (see below for channel distribution), was 68 MΩ and the time constant (τ_{in}) was 35 ms. When a 10 nS somatic (impalement) shunt to resting potential was added, R_{in} and τ_{in} reduce to 42 MΩ and 19 ms, respectively, comparable to the average values reported to have been measured from these cells with sharp electrodes *in vitro* (Mason & Larkman, 1990). No impalement shunt was included in the present study. Compartment equations were integrated forward using a 2-step Runge-Kutte algorithm, and a time step of 4 μs.

Background synaptic inputs

In modelling the background environment we sought to account for the recently reported result (Destexhe & Paré, 1999) that local perfusion of TTX increases R_{in} from an average of 9 MΩ to 46 MΩ in pyramidal cells recorded with sharp electrodes in lightly anaesthetized cats during rapid eye movement episodes. Presumably this increase in R_{in} arose primarily from the elimination of synaptic conductance in the measured cell due to failure of axonal transmission.

We simplified the complexity of the background of synaptic input which impinges upon the 15 000 spines on the layer 5 cell by assuming it was uniformly distributed and constant in time. Active background synaptic contacts had the same density as spines noted above, and were assumed to release at an average background rate of 1 Hz, which might, for example, correspond to a presynaptic invasion rate of 2 Hz and an average probability of release of 50 %. Each such contact incorporated a 1 nS AMPA and 0.25 nS NMDA

Table 1. Background parameters

	Dendritic background			Somatic background		
	AMPA	NMDA[c]	$GABA_A$	AMPA	NMDA[c]	$GABA_A$
Synapse density (contacts μm^{-2})[a]	0.64	0.64	0.10	0	0	0.51[d]
Peak conductance (nS contact^{-1})	1.00	0.25	2.00	—	—	2.00
Background rate (Hz)	1.00	1.00	2.00	—	—	2.00
Duration of conductance (ms)[b]	2.00	40.00	10.00	—	—	10.00
Conductance density (mS cm^{-2})	0.13	0.64	0.38	0	0	2.04

[a] For dendritic background, AMPA/NMDA density corresponds to 2 spines μm^{-2}, with inhibitory density 15% thereof. [b] The duration of a square wave with conductance time integral approximating that of the physiological conductance time course. [c] The NMDA conductance is in the absence of Mg^{2+}. [d] Corresponds to 1000 inhibitory synapses on a spherical soma with 25 μm diameter.

peak conductance, colocalized, both with a 0 mV reversal potential. With these assumptions, background peak AMPA and NMDA dendritic conductance densities were 0.13 and 0.64 mS cm^{-2}, respectively, with the larger NMDA density a result of that channel's much longer open time (Table 1). Desensitization was not incorporated. The NMDA conductance density was gated by voltage in each compartment, and so background NMDA current was spatially non-uniform and dependent on dendritic depolarization (see Discussion). Note that with uniform and constant background individual variables such as active spine density, peak conductance per synapse, average background rate, and duration of conductance are not individually meaningful; what is relevant is only their product, the density of background conductance.

Dendritic inhibitory background was also modelled with a uniform distribution, with inhibitory contact density 15% that of spines, following Destexhe & Paré (1999). Its lower synaptic density notwithstanding, the longer average duration of inhibitory conductance (we assumed a single channel type with a −75 mV reversal and a 10 ms average open time) resulted in comparable inhibitory and excitatory background conductance densities (details in Table 1). The soma was assumed to have 1000 inhibitory and no excitatory synapses, consistent with observed ultrastructure, representing a 5-fold denser inhibitory innervation than that in the dendrites. Though no somatic shunt to resting voltage was used in the study itself, for the purpose of comparing model input resistance with the measurements of Destexhe & Paré (1999), in which sharp electrodes were used, we added a 10 nS somatic shunt to rest. With that in place R_{in} reduced from 42 to 8 MΩ when the background synaptic input was applied in the simulated cell, comparable to the drop from 46 to 9 MΩ they reported. The background reduced the input time constant measured at the soma to about 3 ms.

Na^+, Ca^{2+} and K^+ channel densities in the apical trunk

Simulation of dendritic responses to synaptic input in pyramidal cells requires an accurate distribution of dendritic ion channels, which in turn determine dendritic excitability. Two distributions were utilized, both of which endowed the apical trunk with Na^+, Ca^{2+} and K^+ channels, and in both of which backpropagation of somatic spikes was supported. In Case I dendritic excitability was primarily conferred by the Na^+ channels, while in Case II Ca^{2+} densities were increased sufficiently to enable the distal Ca^{2+} spikes which appear to characterize responses to distal input in cell type (Amitai *et al.* 1993; Schiller *et al.* 1997; Larkum *et al.* 1999*a*,*b*; Zhu, 2000) in relatively mature slices (i.e. older than P28). We wished to compare responses to synaptic input to the apical dendrite with and without these Ca^{2+} spikes present, recognizing that they can be suppressed or modulated under circumstances of physiological relevance.

Na^+ channels

Throughout this study 'conductance density' refers to the conductance per unit area with all channels open, which is the value multiplied by m^3h in standard Hodgkin-Huxley equations. To derive this value from the measured peak current density during a voltage command step, conductance derived using that measurement must be corrected by dividing by the channel open probability at the peak current (about 40% for the Na^+ current). Applying this adjustment, patch electrode measurements along the apical trunk in young (P14) rat layer 5 pyramidal cells suggest Na^+ channels are uniformly distributed with conductance density approximately 10 mS cm^{-2} throughout much of the trunk (Stuart & Sakmann, 1994).

It is, however, problematic to rely on average peak current per patch to derive conductance *density* estimates, since there is uncertainty regarding the membrane area of the average patch (D. Johnston & C. Colbert, personnel communication) by which measured currents are divided to calculate densities. Fortunately, electrophysiological measurement of peak rate of rise during the upstroke of the backpropagating wave measures net inward current per unit capacitance. Since the Na^+ channel is the fastest to open amongst voltage gated channels opening near threshold, peak rate of rise is a good measure of *available* (i.e. non-inactivated) Na^+ channel density (authors' unpublished observations). Indeed backpropagation itself is highly sensitive to the voltage dependence of Na^+ channel inactivation (Rhodes, 1997, 1999), which can alter the density of available Na^+ channels. Thus requiring a simulated backpropagating wave to match the rate of rise measured *in vitro* is a means to calibrate channel density in simulation. Using the amplitude reported by Stuart *et al.* (1997, their Fig. 2) for the backpropagated wave in P28 layer 5 cells from somatosensory cortex, at 35°C, a Na^+ channel density of 12 mS cm^{-2} was required for the simulated backpropagated amplitude to match that measured in the distal trunk. This trunk Na^+ density, uniformly distributed, was used in the Case I density distribution.

More recent layer 5 cell distal trunk data have revealed a falling off of backpropagated amplitude in the most distal trunk (Larkum *et al.* 1999*a*,*b*) in mature cells, a different profile than implied by Stuart *et al.* (1997). While further experimental data will be needed to definitively establish trunk Na^+ density, in the Case II distribution we accounted for the recent data by reducing Na^+ conductance density in a graded fashion from 12 to 8 mS cm^{-2} from the most proximal to the most distal trunk.

While patch measurements of channel densities in the apical oblique branches have not been made, due to the impracticability of attaching patch electrodes to those very small diameter (~0.7 μm) processes, an inference can be drawn from Ca^{2+} imaging data (Yuste *et al.* 1994; Schiller *et al.* 1995), which indicate that somatic firing

Table 2. Channel kinetics

Sodium Channel

$$g = \bar{g}_{Na} \cdot m^2 \cdot h$$

$$\frac{dm}{dt} = -\beta_m \cdot m + \alpha_m \cdot (1 - m)$$
$$\alpha_m = -320 \cdot (V + 46.9) / (e^{(-(V+46.9)/4.0)} - 1)$$
$$\beta_m = 280 \cdot (V + 19.9) / (e^{((V+19.9)/5.0))} - 1)$$

$$\frac{dh}{dt} = (h_\infty - h) / \tau_h$$
$$h_\infty = 1/(1 + e^{(V-(-50.0)/7.0)})$$
$$\tau_h = 1/(\alpha_h + \beta_h)$$
$$\alpha_h = 68.8 \cdot (V + 35.0) / (1 - e^{(-(V+35.0)/5.0)})$$
$$\beta_h = -26.1 \cdot (V + 60.0) / (1 - e^{((V+60.0)/5.0)})$$

Delayed Rectifier

$$g = \bar{g}_{KDR} \cdot n$$

$$\frac{dn}{dt} = -\beta_n \cdot n + \alpha_n \cdot (1 - n)$$
$$\alpha_n = -16 \cdot (V + 24.9) / (e^{(-(V+24.9)/5.0)} - 1)$$
$$\beta_n = 375 \cdot e^{(-(V+40.0)/40.0)}$$

A-Current

$$g = \bar{g}_A \cdot m \cdot h$$

$$\frac{dm}{dt} = (m_\infty - m) / \tau_h$$
$$\frac{dh}{dt} = (h_\infty - h) / \tau_h$$

For Case I channel distribution:

$$m_\infty = 1/(1 + e^{(V-(-1.0)/15.0)})$$
$$\tau_m = 1.25$$
$$h_\infty = 1/(1 + e^{(V-(-56.0)/8.0)})$$

If (V > -63.0 mV) $\tau_h = 6.3$,
otherwise $\tau_h = (0.3/(e^{(V+46.0)/5.0} + e^{(V+23.8)/37.5}))$

For Case II channel distribution, from Bekkers 2000a:

$$m_\infty = 1/(1 + e^{(V-(-17.7)/16.6)})$$
$$h_\infty = 1/(1 + e^{(V-(-72.2)/6.7)})$$

High Threshold Calcium Channel

$$g = \bar{g}_{Ca} \cdot m^2 \cdot h \cdot (1/(1 + [Ca]/0.5\mu M)$$

$$\frac{dm}{dt} = -\beta_m \cdot m + \alpha_m \cdot (1 - m)$$
$$\alpha_m = 1600/(1 + e^{(-(V-5.0)/13.9)})$$
$$\beta_m = 20 \cdot (V + 8.9) / (e^{(V+8.9)/5.0} - 1)$$

$$\frac{dh}{dt} = (h_\infty - h) / \tau_h$$
$$h_\infty = 1/(1 + e^{(V-(-42.0)/8.0)})$$
$$\tau_h = 20.0,$$

K_{Ca} - Calcium-gated potassium channel

$$g = \bar{g}_{KCa} \cdot m \cdot \min(1, ([Ca] - 0.05\mu M)/0.5\mu M)$$

$$\frac{dm}{dt} = -\beta_m \cdot m + \alpha_m \cdot (1 - m)$$

if (V>10.0 mV)

$$\alpha_m = 2000\, e^{(-(V+53.5)/27.0)}$$
$$\beta_m = 0.0$$

if (V<=10.0 mV)

$$\frac{dm}{dt} = -\beta_m \cdot m + \alpha_m \cdot (1 - m)$$
$$\alpha_m = (e^{((V+50.0)/11.0 - (V+53.5)/27.0)})/18.975$$
$$\beta_m = 2000\, e^{-(V+53.5)/27.0} - \alpha_m$$

K_{mAHP} - Calcium-gated medium after hyperpolarizing potassium channel

$$g = \bar{g}_{mAHP} \cdot m \cdot \min(1, ([Ca] - 0.05\mu M)/2.5\mu M)$$

$$\frac{dm}{dt} = (m_\infty - m) / \tau_m$$

$$\tau_m = 39.7$$

for V ≤ -54, $m_\infty = 0$

for V > -54 and < -40, $m_\infty = (V + 54)/14$

for V ≥ 40, $m_\infty = 1$

propagates into these branches. Since dendritic Ca^{2+} channels do not sustain propagation (Rhodes, 1999), this suggests that Na^+ conductance is present in the branches at densities adequate to sustain that invasion. Simulations indicate the minimum dendritic Na^+ conductance density necessary to support invasion of the side branches is 3–4 mS cm^{-2} (authors' unpublished simulation observations), setting a lower bound on Na^+ density there. In both Cases I and II, Na^+ conductance density of 6 mS cm^{-2} was included in the oblique branches. In order to be conservative with respect to simulated tuft excitability we incorporated just 2 mS cm^{-2} in tuft membrane, the low end of the plausible range. Details of channel distributions are provided in Tables 2 and 3.

K^+ channels

In addition to dendritic Na^+ channels, a fast delayed rectifier (K_{DR}) was included at about half the Na^+ conductance density (details in Table 3). Its activation threshold, about −30 mV, was well above the threshold for triggering local Na^+-propagated excitation in the trunk (which was between −48 and −43 mV). We therefore do not expect the results to qualitatively depend upon K_{DR} density.

In contrast, the A-current activates at low voltages and so may play an important role in controlling synaptic integration and the initiation of regenerative activity in pyramidal cell dendrites (Andreason & Lambert, 1995). In the Case I distribution A channel conductance was uniformly distributed at 3 mS cm^{-2}, while in Case II it was tapered from 2 to 4 mS cm^{-2} from proximal to most distal trunk, matching the densities implied by Bekkers's recent measurements (Bekkers, 2000*a*,*b*; and J. Bekkers, personal communications). The kinetics are detailed in Table 3. Because cells in Bekkers (2000*a*,*b*) were relatively young (P14–22), it seems plausible that as data from more mature cells becomes available the A-current density in distal trunk might further increase (Hamill *et al.* 1990), with consequences for synaptic integration of distal inputs which remain to be examined.

In Case II, where dendritic Ca^{2+} channels were prominent, the fast and medium rate [Ca^{2+}]- and voltage-gated K_{Ca} and K_{mAHP} channels which occur in layer 5 cells (Schwindt *et al.* 1988) were increased and added, respectively, in the dendrites to provide control of Ca^{2+} spikes. Full [Ca^{2+}] gating was reached at [Ca^{2+}] of 1 mM (K^+ channel kinetics and [Ca^{2+}] gating formulae in Table 3). Since no data are available on the dendritic densities of these channels, their density was set at the minimum needed to provide enough control of dendritic Ca^{2+} events to preserve physiological somatic responses to somatic current step. A 4 mS density for both channels, uniformly distributed through the apical dendrite, was adequate to provide this control.

Ca^{2+} channels

Optical data regarding dendritic Ca^{2+} influx (Yuste *et al.* 1994; Schiller *et al.* 1995) indicate that all pyramidal cells, including both bursting and regular spiking subtypes (Rhodes *et al.* 1995), incorporate dendritic high threshold Ca^{2+} channels throughout the dendritic tree. In the Case I dendritic channel distribution, an L-type Ca^{2+} channel was incorporated at low density (2 mS cm^{-2}) only in the apical trunk, accompanied by 1 mS cm^{-2} of K_{Ca} (details in Tables 2 and 3). This distribution produced measurable Ca^{2+} influx into the trunk during backpropagation, but not distal Ca^{2+} current-driven events. Calcium concentration was governed by a first order kinetic system including two fully mixed buffers, one fast and one slow, the details of which are provided in Rhodes & Gray (1994).

While reports from relatively immature layer 5 cells (e.g. Stuart & Sakmann, 1994, P14) evidence an apical trunk dominated by Na^+ currents, measurements of electrical responses in the distal trunk of more mature layer 5 cells (Amitai *et al.* 1993; Schiller *et al.* 1997; Stuart *et al.* 1997; Seamans *et al.* 1997; Larkum *et al.* 1999*a*,*b*; Zhu, 2000) reveal the generation of Ca^{2+} spikes in the apical dendrite, presumably the result of a higher density of dendritic Ca^{2+} channels in the more mature cells. For the Case II model cell, we utilized a dendritic Ca^{2+} channel density distribution which exhibited the distal Ca^{2+} events in the apical dendrite which have been found to characterize responses in more mature cells. In this case Ca^{2+} conductance in the trunk was increased to 5.3 mS cm^{-2}, with 2.6 mS cm^{-2} in the oblique branches. This non-inactivating current drove a depolarizing plateau in the distal apical dendrite, lasting approximately 20–30 ms, which was terminated in part by [Ca^{2+}]-gated K^+ current (Rhodes & Gray, 1994). To be conservative with respect to the intrinsic excitability of the tuft, as with Na^+ channels (see above) the lowest Ca^{2+} channel density, 1.3 mS cm^{-2}, was included in that region.

Channel conductance densities in the cell body and axon

Na^+ density in the soma and abutting axon was set to the same value in accordance with comparison of their densities in both subicular (Colbert & Johnston, 1996) and layer 5 (Stuart *et al.* 1997) pyramidal cells. This value was set by requiring that together the Na^+ currents in these elements drive the somatic action potential rate of rise. Somatic and axonal Na^+ density of 100 mS cm^{-2} along with 40 mS cm^{-2} in the short thick dendritic segments abutting the cell body drove somatic action potentials with the 500 V s^{-1} upstroke and 100 mV amplitude measured in this cell type *in vitro* (McCormick *et al.* 1985). A 100 mS cm^{-2} axonal density was adequate to ensure secure propagation of somatic firing along the axon. This density is much lower than that which has often been utilized in the initial segment in modelling studies (e.g. Mainen *et al.* 1995), but our results confirm that even with a uniform Na^+ density in the soma and axon, axonal initiation occurs in response to threshold proximal inputs.

Table 3. Channel Distribution. Case I: apical dendrite supports Na^+-mediated backpropagation but not Ca^{2+} spikes; and Case II: apical dendrite supports both Na^+-mediated backpropagation and Ca^{2+} spikes

	Case I			Case II		
	Trunk	Branches	Tuft	Trunk	Branches	Tuft
Na	12	6	2	12 to 8*	6	2
K_{DR}	4.5	3	1	4.5	3	1
K_A	5	3	3	2 to 4*	3	3
Ca	2	0	0	5.3	2.6	1.3
K_{Ca}	1	0	0	4	4	2
K_{mAHP}	0	0	0	5	4	2

* The range refers to a gradient of density in the apical trunk from soma outward (see Methods for rationale). All channel conductance densities are expressed in mS cm^{-2} and assume open probability at 100 %.

Simulated patterns of apical synaptic input

The response characteristics of active dendritic trees depend upon the spatiotemporal pattern of inputs chosen. For example, in dendrites with voltage-gated depolarizing current a concentrated input can trigger intrinsic currents which would not be invoked with a more dispersed pattern containing the same synaptic conductance (Mel, 1994). Accordingly, in attempting to usefully characterize the efficacy of inputs to the layer 5 pyramidal cell apical dendrite, one wishes to utilize patterns of synaptic stimuli with some physiological relevance. The form of input chosen was a 30 Hz train of synaptic conductances applied to a set of dendritic segments in either the apical tuft or in the apical oblique branches, target areas chosen to roughly correspond to layer 1 or layer 4 axonal input patterns. The efficacy of this synaptic input was assessed over a 150 ms stimulation period comprising five input barrages. When background synaptic conductance was applied, the simulated cell was given 20 ms to reach equilibrium voltage throughout the dendritic tree before the 150 ms stimulus train commenced. Synaptic conductances were a mixture of AMPA and NMDA (comprising 80 % and 20 % of peak conductance, respectively) (kinetics in Table 2), with 0 mV reversal potentials. Unless otherwise specified, conductance magnitudes in this paper refer to the AMPA component peak conductance only, with the assumption that NMDA conductance was always colocalized at peak level one-quarter that of the AMPA component.

The magnitude of the input applied to these distal and proximal synaptic stimulation areas was systematically varied to characterize the cell's response as a function of the relevant variables. In each instance, we wished to know the threshold levels at which the proximal or distal input by itself triggered firing, and the spatiotemporal patterns of initiation and subsequent regenerative activity elicited by these inputs. Arrival times amongst the segments

receiving input within either the tuft or the proximal apical target zone were always coincident. Model variations examined but not reported here included doubling the number of segments over which a given total input was distributed, elimination of NMDA conductances by increasing model [Mg^{2+}] to 100 mM, increase in proximal apical trunk density from 12 to 20 mS cm^{-2}, downregulation of the A-current by a 15 mV rightward shift in the voltage at which 50% steady state activation of the A-channel is reached (Hoffman & Johnston, 1998), and elimination of apical tuft Na^+ density. The conclusions reached in this paper were robust to these variations in the parameters we used.

Spatiotemporal plots of voltage along the apical axis

During each simulation, the sites of initiation and the subsequent spatiotemporal evolution of regenerative activity in the cell was monitored along the apical trunk, soma and axon during simulations. As will be described, this process was more complex than expected, with, for example, the site of initiation changing as an identical input was repeated. Conventional voltage traces selected from individual compartments often failed to capture this complexity. In order to better record and report this history, we used a spatiotemporal plot in which voltage in each compartment of the axis from axon and soma through the 15 compartments of the simulated apical trunk was encoded as a colour and painted on a two-dimensional plot as a function of distance from the soma (the ordinate) and of time (the abscissa). This spatiotemporal voltage plot enabled a complete record of the history of voltage along the entire axis to be examined at a glance, capturing the site or sites of initiation, and the manner in which firing propagated.

RESULTS

We examined synaptic responses of the model layer 5 cell to synaptic input to the apical tuft and to proximal apical branches in two simulated background conditions, the first more analogous to the case in cortical slices, where much of the available data on neuron intrinsic properties and synaptic physiology is gathered. In this case no background synaptic conductance was applied. In the second case responses to the same synaptic inputs were assessed when overlaid upon a uniform synaptic background intended to better simulate the *in vivo* environment (see Methods).

Responses of layer 5 cells in the absence of synaptic background

In the following, 30 Hz trains of synaptic input were used, and efficacy quantified as the somatic firing rate during a 150 ms period of input barrages.

Synaptic inputs to the proximal apical dendrite: subthreshold response characteristics

A small synaptic input to proximal apical oblique branches, approximately 3 nS peak AMPA conductance applied to each of five branches receiving input (Fig. 1*A*), was sufficient to trigger branch spikes 70 mV in amplitude in the targeted oblique branches (Rhodes, 1999). These events

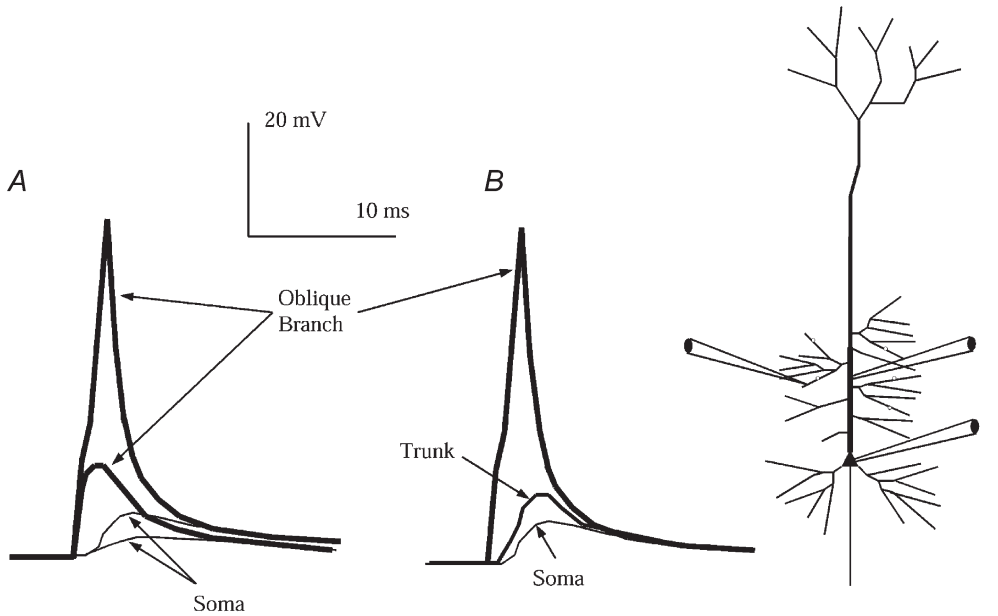

Figure 1. Small inputs trigger isolated branch spikes which boost the subthreshold somatic EPSP

A, the responses to small inputs applied to the 5 apical oblique branch segments shown (small circles in this and subsequent figures indicate locations and magnitude of synaptic conductances). A 3 nS (peak AMPA) conductance triggered branch spikes 70 mV in amplitude in the targeted oblique branches, whereas a 2 nS input elicited a largely passive response in the branch (oblique branches plotted with thickest traces). The branch spike was driven by dendritic Na^+ current, and was all-or-none in that once triggered its amplitude was not determined by synaptic input. Though isolated in the branches, the branch spikes boosted the somatic EPSP (thinnest traces) from about 2 to 5 mV (arrows). *B*, the response to 3 nS shown again, here with the voltage in the apical trunk (intermediate trace) adjacent to target oblique branches. Firing in the branches failed to propagate into the apical trunk notwithstanding its higher density of Na^+ channel conductance in this simulation (12 in the trunk *vs.* 6 mS cm^{-2} in the side branches).

were driven by dendritic Na^+ current, and were all-or-none (Kuno & Llinás, 1970) in that once triggered their amplitude was not determined by synaptic input. Though isolated in the branches (Rhodes, 1999), these branch spikes boosted the somatic EPSP with respect to the EPSP produced by input just under branch firing threshold, from about 2 to 5 mV (arrow, Fig. 1*A*). Note that events in the branches failed to propagate into the apical trunk (Fig. 1*B*) notwithstanding its higher density of Na^+ channel conductance in this simulation (12 in the trunk *vs.* 6 mS cm^{-2} in the side branches), a result of the load mismatch between the thick trunk and finer branches.

Stronger inputs triggered firing in sub-branches adjacent to those receiving the input with a few milliseconds delay, with the secondary firings appearing as distinct shoulders in the declining phase of the voltage trace of the primary recipient branch. The oblique branch firings often caused an irregular bumpy appearance (Fig. 2) measured in the trunk near the sites of input. To our knowledge these features in trunk impalement voltage records have not previously been reported. If in future electrophysiological experiments it becomes feasible to selectively stimulate oblique branches, we expect the presence or absence of these voltage bumps at the trunk will ascertain whether the predicted excitability in oblique branches occurs under experimental conditions.

As inputs approached threshold, the spatiotemporal plot revealed the beginnings of axonal initiation: peak voltage in the axon initial segment (IS), though subthreshold, rose above that in the soma during the EPSP (Fig. 2, arrow). This occurred despite the density of Na^+ channels in the IS and soma being identical in our model (Colbert & Johnston, 1996; Stuart *et al.* 1997), and is a precursor of axonal initiation.

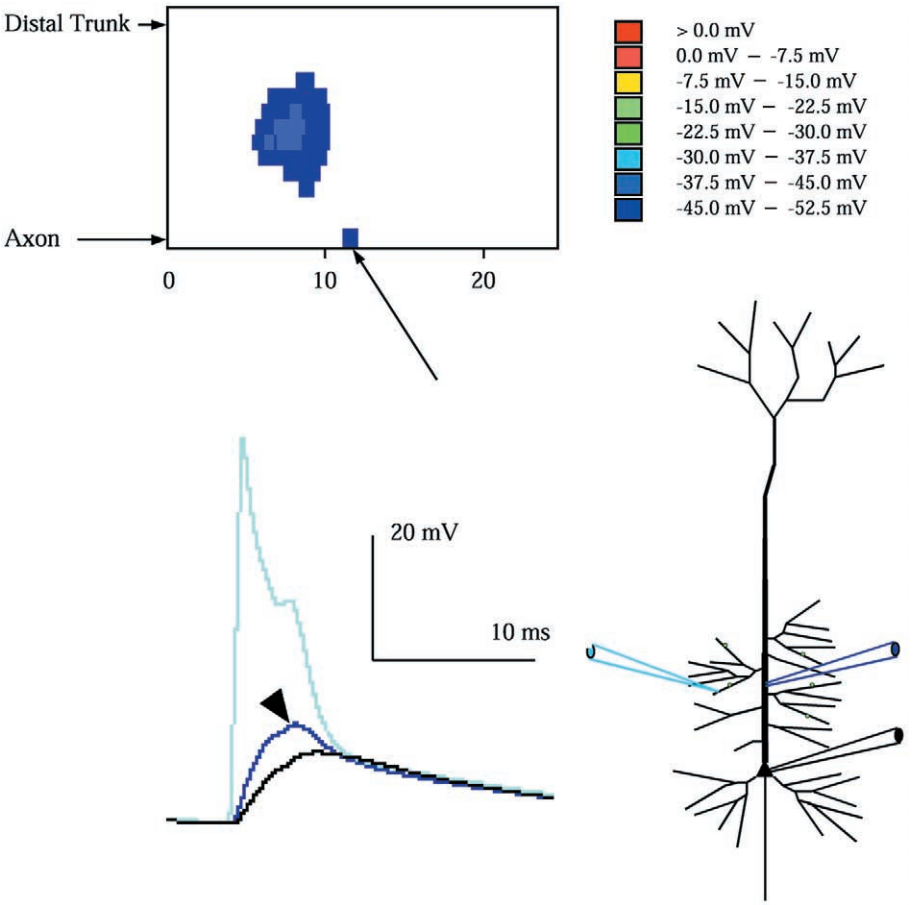

Figure 2. Strong subthreshold input reveals the events preceding axonal initiation

Strong subthreshold inputs (12 nS to each branch, 60 nS total) can recruit adjacent branches not receiving input. Firing was triggered in adjacent sub-branches with a few milliseconds delay, the effect of which appeared as bumps in the voltage trace (arrowhead) measured in the trunk near the sites of input. The spatiotemporal plot, which records the voltage history along the entire axo-somato-dendritic axis (see Fig. 3 for the mapping between the ordinate of the spatiotemporal plot and the axis it represents), reveals a subthreshold event which precedes axonal initiation: peak voltage in the axon initial segment (arrow), though subthreshold, exceeds that in the soma during the EPSP. In this and subsequent plots, voltage is coded in colour as shown. The time scale for the spatiotemporal plot is the same as for the voltage trace, and they are in register.

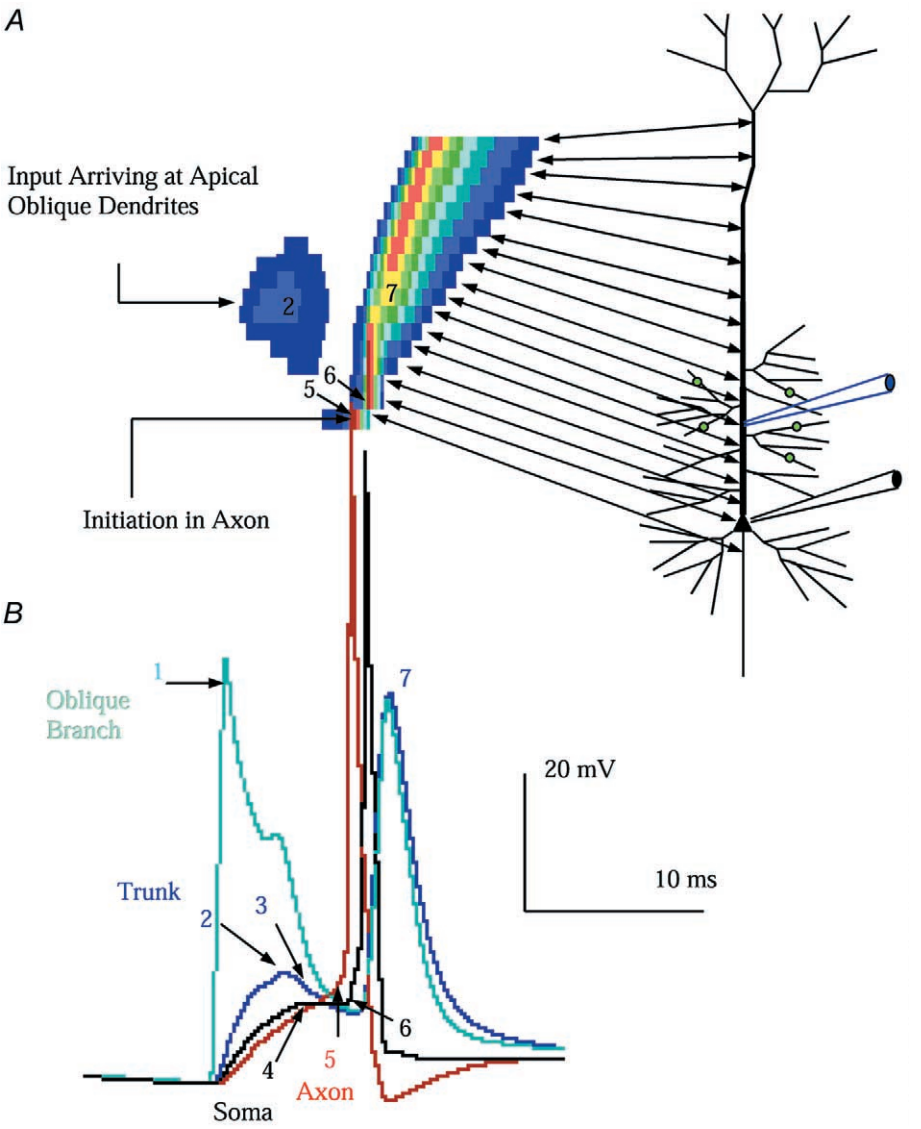

Figure 3. Threshold input to proximal apical branches triggers initiation in the axon, even if the Na^+ conductance density in the axon and soma are equal

A, spatiotemporal plot of the threshold sequence of events. The two-headed arrows indicate the correspondence between the ordinate of the spatiotemporal plot and location along the axo-somato-dendritic axis. The numbers correspond to the spatiotemporal location of some of the numbered points on the traces. The spatiotemporal location of initiation is indicated. *B*, in the absence of background, when input reached 13 nS per branch, 65 nS total, the second barrage triggered initiation in the axon with subsequent somatic firing and backpropagation. The following sequence of events was observed (numerals refer to arrow numbers in the figure): (1) The synaptic input triggered firing in the branches receiving input. (2) Voltage in the adjacent apical trunk rose to a peak of 12 mV, before (3) beginning to repolarize. After a several millisecond delay, (4) voltage at the soma and proximal axon approached threshold, about −55 mV. (5) Axonal voltage accelerated ahead of the soma, with firing initiating in the proximal axonal segment, followed by the soma. Note the sharp 90 deg inflection in the somatic trace (6) indicating the impact of the axon firing accelerating the rise of somatic voltage. Following somatic firing, an Na^+ channel-dependent voltage wave propagated outward through the apical dendrite (Rhodes & Gray 1993; Stuart & Sakmann 1994), (7) arriving in the apical trunk during the downslope of the EPSP as observed *in vitro*. The red trace is the proximal axon, the blue trace is the trunk, the teal trace is an oblique branch receiving input, and the black trace is the soma.

The sequence of events leading to axonal initiation following threshold input to the proximal apical dendrite

When the proximal apical input reached about 65 nS in total the second input barrage triggered the following sequence of events (Fig. 3).

(1) Synaptic input triggered branch firings in the oblique dendrites receiving input. Voltage in the adjacent trunk rose about 12 mV above rest but began to repolarize (arrows 2 and 3 in Fig. 3).

(2) As the synaptic depolarization passively spread inward and Na^+ firing threshold (about −55 mV) was approached at the soma, the rate of change of voltage in the proximal axon (arrow 4) began to outpace the soma, notwithstanding the uniformity of Na^+ channel densities and membrane capacitance in soma and axon. This presumably occurred because input impedance in the axon is much higher, and so given identical initial Na^+ current density, charge-up of the membrane capacitance occurs more quickly there. Thus a super-concentration of Na^+ channel density in the axon IS (cf. Mainen *et al.* 1995) is not required to account for the axonal initiation observed in layer 5 pyramidal cells following moderate proximal input (Stuart *et al.* 1994). The sharp 90 deg upstroke of the action potential in the soma (arrow 6) is a signature indicating that somatic currents did not initiate the somatic action potential.

(3) Following somatic firing, a Na^+ channel-dependent voltage wave propagated outward through the apical dendrite (Rhodes & Gray, 1993; Stuart & Sakmann, 1994), arriving in the apical trunk during the downslope of the EPSP there. The velocity of the backpropagating wave peak was ∼0.2 m s^{-1}, and it travelled from soma to the base of the apical tuft in 3.5 ms. The spatiotemporal plot allows a visual assessment of the site of initiation, along with the direction, speed, and duration (width on the x-axis) of the backpropagating wave as it travelled outward through the apical trunk.

Shifts in the site of initiation with repeated identical input

As voltage along the apical trunk built up from repeated input, however, the initiation region shifted (Zecevic &

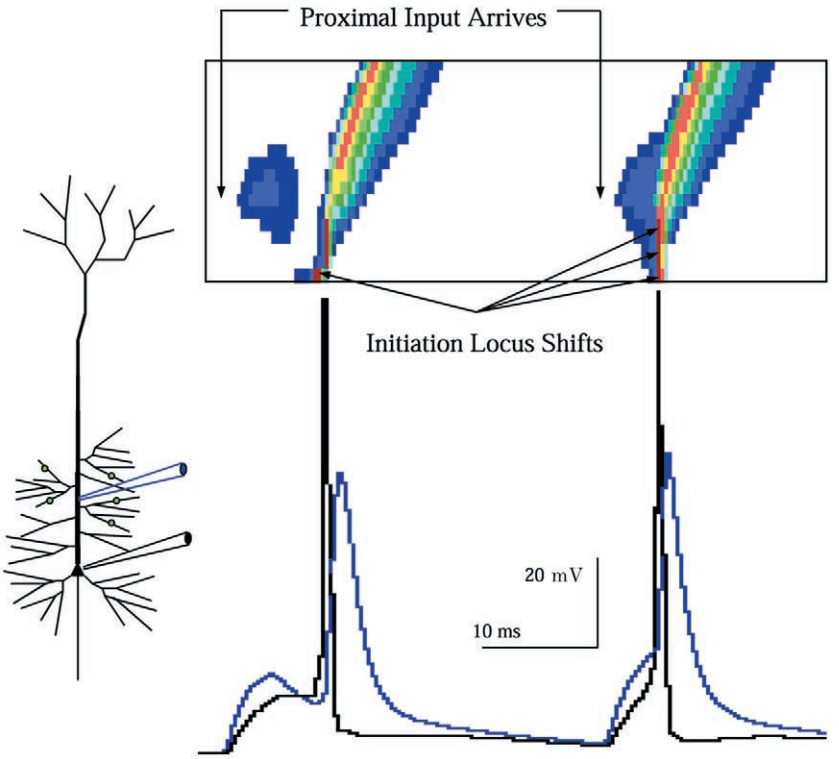

Figure 4. Shifts in the site of initiation with repeated identical input

The same input as in Fig. 3, with the response to the next input barrage included for comparison. With the subsequent (identical) barrage the initiation region shifted. Whereas in the first response (cf. Fig. 3) initiation was in the axon, the following barrage caused the site of initiation to both shift and spread out. The spatiotemporal plot makes it clear that with the latter input firing initiated simultaneously throughout a tract of membrane in the apical trunk stretching from the site of input to the soma. Here the notion of a single 'initiation site' gives way to an extended 'initiation zone'. Stronger inputs led to increasingly distal and spatially focal initiation closer to the site of the input (not shown).

Antic, 1998). With threshold input the second barrage triggered initiation in the axon as just described, but the third barrage triggered initiation of firing near-simultaneously across a tract of membrane in the apical trunk stretching from the site of input to the soma (Fig. 4). In this instance the notion of a single 'initiation site' is not applicable, and there is of course no causal primacy regarding firing in the IS. Indeed, we commonly found that the site of initiation was dynamic, shifting as the voltage history and inactivation state of the Na^+ channels in the trunk evolved during activity, with simultaneous initiation along a considerable section of the apical trunk a very typical form of initiation under a variety of stimulus conditions. These observations suggest that the notion of the axon IS as a master summation zone which renders a firing 'decision' seems to apply in only a limited set of circumstances, as suggested by current source density observations of CA1 pyramidal cell initiation following Schaffer collateral stimulation (Richardson *et al.* 1987).

Higher amplitude proximal input (results not shown) led to an increasingly focal point of initiation adjacent to the site of the input (Turner *et al.* 1991).

The inclusion of dendritic Ca^{2+} spikes did not affect the mechanisms of initiation following proximal synaptic input

Impalements of the distal apical trunk of relatively mature (approximately P28 or older) layer 5 cells indicate that dendritic Ca^{2+} spikes are readily produced in response to distal input (Amitai *et al.* 1993; Schiller *et al.* 1997; Stuart *et al.* 1997; Larkum *et al.* 1999*a*,*b*; Zhu, 2000). These powerful events can drive the bursts of somatic spikes which characterize intrinsically bursting layer 5 pyramidal cells (McCormick *et al.* 1985; Rhodes & Gray, 1994), and may alter the synaptic integration of distal input. To re-assess synaptic integration in this context the same patterns of input utilized above were re-applied to a model cell in which dendritic Ca^{2+} channel densities supported distal Ca^{2+} spikes (details in Methods).

For the proximal pattern of input, threshold for initiation decreased from 65 to 38 nS (aggregate peak AMPA synaptic conductance), primarily due to the contribution of additional Ca^{2+} currents in the oblique branches activated by the synaptic input. However, the sequence of events underlying initiation of regenerative activity at threshold input was unchanged. The oblique

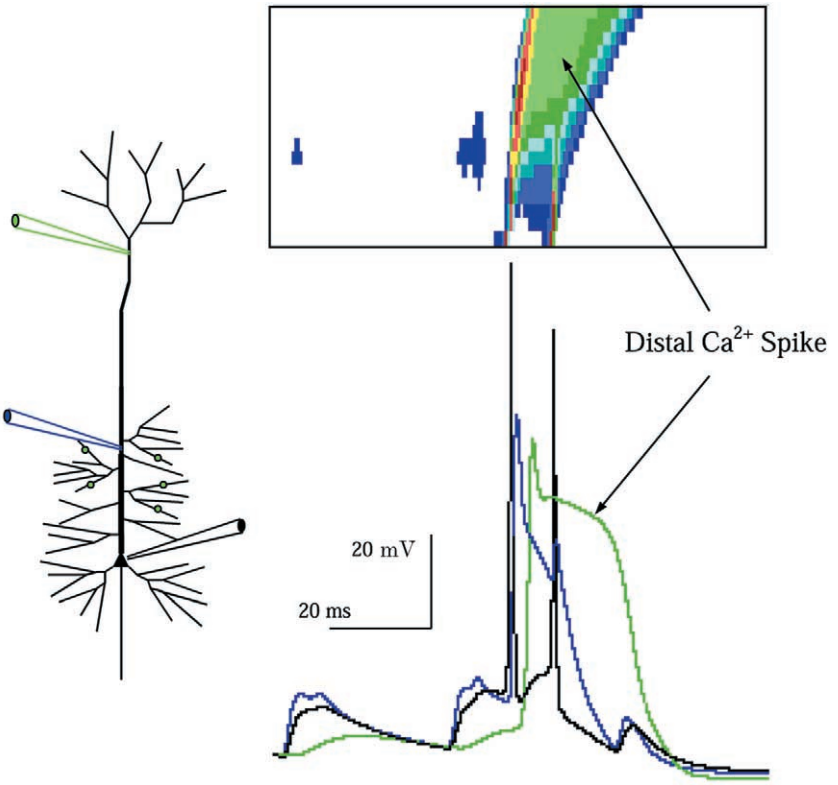

Figure 5. The distal Ca^{2+} spike is not causally related to initiation following proximal input

The response of a model neuron with increased dendritic Ca^{2+} conductance to synaptic input to proximal oblique branches. Here, threshold input is applied. The sequence of events leading to initiation in the axon is identical to that in the model cell when dendritic Ca^{2+} spikes were absent (cf. Fig. 3). Note that the distal Ca^{2+} spike follows initiation, and so is not causally involved. The Ca^{2+} current driven plateau itself drives the soma to fire a second spike, the beginning of an intrinsic burst (Rhodes & Gray 1994).

branches receiving input fired, triggering their neighbours which did not receive input directly. This excitation drove a depolarization of the trunk which in turn spread toward the soma, with initiation occurring in the proximal trunk or in the proximal axon at the threshold level of input. Following initiation a voltage wave backpropagated outward through the distal dendritic tree, triggering a Ca^{2+} current-driven plateau there lasting about 20 ms (Fig. 5). This plateau in turn drove a second somatic spike (Rhodes & Gray, 1994). We found that increasing dendritic Ca^{2+} conductance extended the plateau, enabling distal input (Kamondi *et al.* 1998; Zhu & Connor, 1999) to trigger the multi-spike intrinsic burst characteristic of this cell type (McCormick *et al.* 1985; Helmchen *et al.* 1999; Larkum *et al.* 1999*b*; Zhu & Connor, 1999; Zhu, 2000). Note that in this example with proximal synaptic input the dendritic Ca^{2+} event *followed* initiation and so did not play a causal role in triggering firing.

Dendritic Ca^{2+} accumulation in the aftermath of the dendritic Ca^{2+} spike required ~80 ms to dissipate with the Ca^{2+} buffering and pump kinetics we utilized, a recovery time not inconsistent with optical measurement of dendritic [Ca^{2+}] recovery following influx from voltage-gated Ca^{2+} channels (Schiller *et al.* 1995; Helmchen *et al.* 1996). During this [Ca^{2+}] recovery period we found that the efficacy of further synaptic input to the apical dendrite was suppressed by dendritic Ca^{2+}-gated K^+ currents. Even strong input, 300 % of threshold, did not cause subsequent cell firing until dendritic [Ca^{2+}] recovered (result not shown), imposing a low pass filter upon synaptic input via the activation of dendritic K^+ currents during the [Ca^{2+}] recovery period. This prediction and its dependence upon the densities and properties of dendritic Ca^{2+}-gated K^+ currents, about which little is known, were not further examined.

Synaptic input to the apical tuft in the absence of background

We next examined the effect of input to the apical tuft, again applying a 30 Hz train of inputs to five separate dendritic segments, increasing synaptic conductance incrementally until threshold was reached.

Subthreshold inputs cause branch firing isolated to the tuft

As with apical oblique branches, the high impedance of tuft terminal branches enabled a small input, 2.5 nS peak AMPA conductance per segment representing perhaps a handful of simultaneously releasing terminals, to drive voltage past activation threshold for a regenerative Na^+ current-driven spike in the recipient sub-branch. This was the case (results not shown) even under conditions where input impedance in the distal trunk and first tuft branches was low, as has been reported (Zhu, 2000; see Discussion). Further, the facility of tuft terminal branches to initiate a local spike remained evident even with a rather low density of Na^+ channel conductance (2 mS cm^{-2}) in the simulated apical tuft membrane (*versus* 6 mS and 12 mS in the oblique branches and trunk, respectively; see Methods). The tuft branch spikes reached −15 mV, 56 mV above rest, but at this level of total input the branch events remained relatively isolated to the tuft, and had negligible impact on somatic voltage (Fig. 6, left plot). Thus when propagation from the tuft into the trunk failed large voltage transients in tuft branches had little effect elsewhere in the cell.

Tuft input triggers initiation of firing in the distal apical trunk, which propagates inward to fire the cell

Threshold layer 1 input was just 20 nS. The sequence of events leading to somatic firing was as follows (Fig. 6, right). (1) Excitation spread from the branches receiving input to abutting branches which did not, with secondary excitation occurring following a 3–4 ms delay. (2) Firing in tuft branches did not propagate into the trunk. Instead, depolarization in the tuft was sustained (Fig. 6, right; duration indicated by two-headed arrow in spatiotemporal plot) and so drove an axial ohmic current into the distal trunk. (3) This axial drive charged up the distal trunk to Na^+ threshold (−43 mV in this example). (4) Once a regenerative event initiated there, the Na^+ spike in the distal trunk readily propagated to the soma.

The foregoing outline indicates that the critical event resulting in somatic firing following layer 1 input was initiation of regenerative excitation in the distal trunk, and that tuft depolarization acts by charging up this section of the trunk to firing threshold. Surprisingly, the capability of layer 1 input to fire the cell did not require active membrane properties in the tuft. Indeed, even when tuft branches were made passive, a similar sequence of events led to somatic firing with modest (~15 %) increase in required input (not shown). Rather it was the geometry of the tuft, which favours sustained depolarization and concentrates the effect of many branches at a single nexus, that generates the drive which causes initation in the distal trunk.

The process of integration and initiation of the firing event in the distal trunk took a total of 6 ms, with another 3.7 ms to traverse the 725 μm from base of the tuft to the soma, a velocity of 0.2 m s^{-1}. Thus somatic firing occurred about 10 ms after arrival of the barrage of synaptic input. The pause in latency between tuft and trunk firing indicated that tuft excitation did not smoothly propagate to the trunk; rather, the sustained depolarization of the tuft built up voltage in the trunk over a 6 ms period. In this example threshold for initiation by layer 1 input was less than one-third that (65 nS) required to elicit firing from the more proximal branches. This is noteworthy both because of the tuft's much greater distance from the soma (725 *vs.* 140 μm) and because in this simulation the tuft membrane was chosen to be relatively unexcitable, incorporating a 2 mS cm^{-2} Na^+ conductance density, rather than 6 and

12 mS cm^{-2} in the oblique branches and trunk, respectively. When tuft Na^+ conductance density was increased to that in the oblique branches, its advantage in efficiency of integration was enhanced further (results not shown).

Effects of Ca^{2+} spikes in the apical dendrite on the integration of input to the apical tuft

Synaptic integration to the tuft was re-examined in the context of a more mature dendritic channel distribution with Ca^{2+} current densities increased sufficiently to support distal Ca^{2+} spikes (the Case II dendritic channel distribution in Table 3). In order to remain conservative with respect to the excitability of tuft input in this case, Ca^{2+} and Na^+ conductance densities in tuft membrane were one-half those in the oblique branches, and about one-quarter that in the trunk (see Methods).

The sequence of events leading from distal input to initiation of firing at the distal nexus was altered by the enhanced dendritic Ca^{2+} conductance. Synaptic input to the tuft caused tuft branch spikes which did not propagate inward, but rather which charged the tuft. The depolarized tuft in turn drove initiation of an Na^+-led Na^+–Ca^{2+} spike

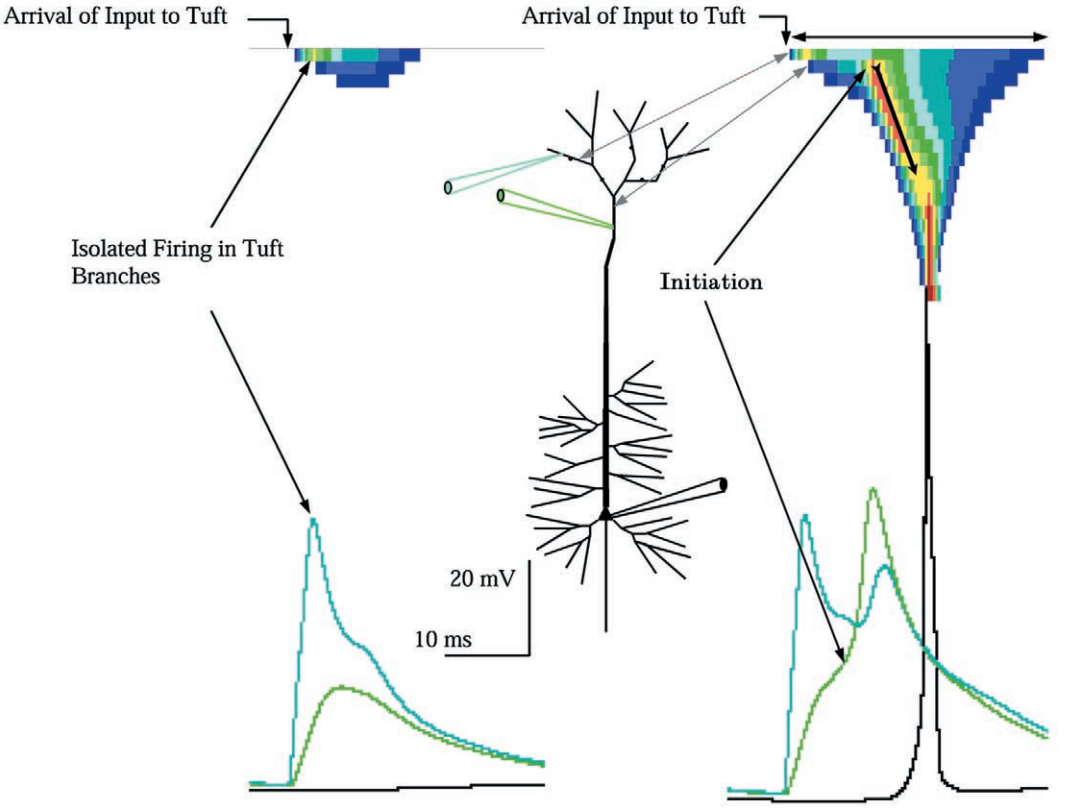

Figure 6. Input to the apical tuft in the absence of background

Left, just-subthreshold input. Just 2.5 nS per branch was adequate to trigger branch excitation, with the Na^+-driven branch spikes reaching −15 mV. Note that despite the full blown event in the tuft branches firing was not triggered in the distal trunk, propagation inward to the soma did not ensue, and the tuft input was almost unobservable in the distal trunk. Right, threshold input to the apical tuft. With a small increase in input, to 4 nS per branch (20 nS total) firing spread from the sub-branches receiving input to abutting unstimulated sub-branches, similar to the spread within apical oblique branches, causing a bump in the declining phase of the voltage trace. The spread of excitation within the tuft and its closed end electrotonic geometry contributed to a rather sustained depolarization there, which in turn provided a sustained drive to the distal trunk, which after a delay for its charge-up reached its firing threshold at −43 mV (arrow). The delay between tuft and trunk indicated that excitation did not propagate from tuft into trunk, but rather that the tuft charged up the trunk over a period of 3–4 ms. The firing of the apex of the trunk was the critical event for firing the cell, because once initiated in the trunk propagation commenced inward, firing the soma when it arrived. Note the relatively abrupt upstroke of the action potential in the soma, a signature of the arrival of an inwardly propagating wave. The spatiotemporal plot reveals that the duration of depolarization in the tuft was quite sustained (two-headed arrow). This sustained tuft depolarization caused a sustained axial ohmic current flow into the distal trunk, which in turn drove voltage in the trunk section abutting the tuft to its Na^+ threshold. Once initiated, the propagation inward proceeded (arrow with tail). Note the narrowing of the temporal (x-axis) width of the dendritic voltage wave as it propagated inward toward the soma.

in the distal apical trunk (Larkum *et al.* 1999*b*) (Fig. 7); this regenerative event propagated inward, firing the soma.

Increased Ca^{2+} channel density in the apical dendrite decreased threshold level of input to the tuft adequate to trigger somatic firing to just 15 nS; thus the efficacy advantage enjoyed by synaptic input to the tuft remained. Since the dendritic Ca^{2+} spike was led and triggered by a regenerative Na^+ event in the distal trunk, the causal sequence of events which led to initiation was essentially the same in both Na^+-dominated ('immature') and Na^+–Ca^{2+} spike competent ('mature') cells.

Responses in the presence of synaptic background

In contrast to the relative absence of background inputs in brain slices, the degree of background synaptic conductance present *in vivo* has been predicted (Holmes & Woody, 1989; Bernander *et al.* 1991) to alter effective membrane resistance and thus the time constant of pyramidal cells awash in background input, a prediction recently confirmed *in vivo* using local perfusion of TTX to reversibly block local axonal transmission (Destexhe & Paré, 1999). We therefore sought to re-examine the effects of synaptic inputs to the apical dendrite in the presence of physiologically plausible simulated background input. To do so we added a uniform density of synaptic background conductance, both excitatory and inhibitory, to all dendritic compartments, along with inhibitory inputs to the soma (details in Methods). Background rates were chosen to produce the 4- or 5-fold reduction in input resistance reported following local perfusion of TTX applied *in vivo* (Destexhe & Paré, 1999).

When this excitatory/inhibitory background was 'turned on', within about 10 ms a new equilibrium potential was reached throughout the cell, ranging from −68 mV in the soma to −62 mV in the distal dendrites.

Responses to apical tuft input when uniform background is present

We re-examined the efficacy of apical tuft input when applied while the background was present. While it may have been expected that the dendritic membrane leakage caused by the background conductances would reduce the comparative advantage of the distant tuft inputs, the opposite was true. The responses to layer 1 input were as follows.

(1) Synaptic inputs up to 2.5 nS per branch were subthreshold for Na^+ channel activation in the target

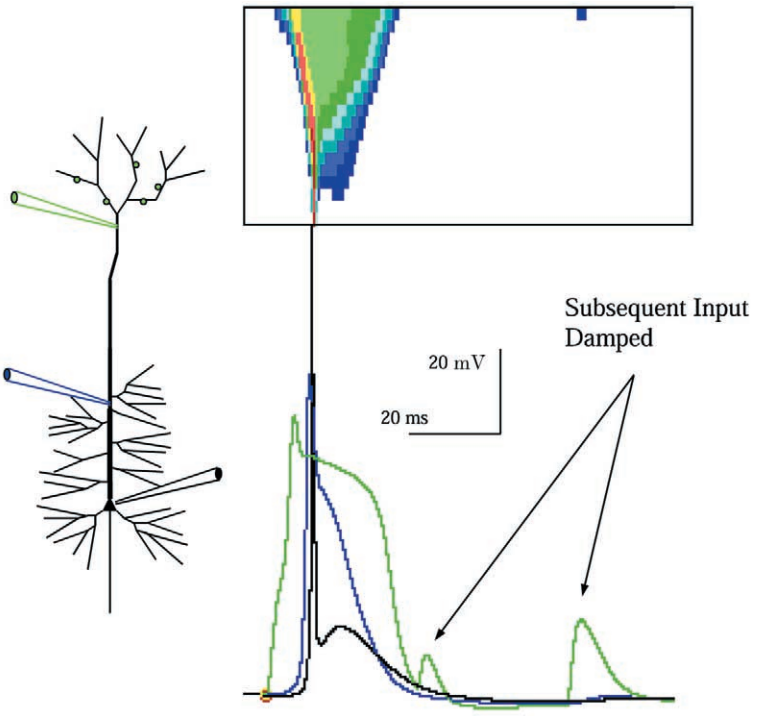

Figure 7. Tuft input triggers a distal Na^+–Ca^{2+} spike which propagates inward

The response of a model neuron with increased dendritic Ca^{2+} conductance to synaptic input to apical tuft branches, in the absence of background. The Ca^{2+} current-driven width of the inwardly propagating voltage wave is greatest most distally and tapers as it travels inward, as can be seen in the spatiotemporal plot. Note that following the Ca^{2+} event subsequent input barrages were less effective in triggering firing. This suppression was due to dendritic [Ca^{2+}]-gated K^+ currents, and wore off with the same time course as Ca^{2+} recovery. As a result, for a 80–100 ms period following a distal Ca^{2+} event, repeated input was ineffective in driving the cell. Note that under these conditions (i.e. in the absence of background) the distal depolarization drives a pronounced after-depolarizing potential in the soma.

branch, but still could elicit large voltage transients due to the high impedance of these recipient branches (Fig. 8, left). In this regime, the EPSP as measured in the distal trunk remained small (no more than 7 mV) and the effect at the soma was negligible.

(2) At 2.5 nS input per branch the synaptic current triggered a Na^+-driven regenerative spike in the branch reaching about −22 mV, about 40 mV above the resting potential in the tuft in the presence of background. Thus the peak voltage reached during this event was 7 mV less than that when background was absent, as a result of the resting inactivation of Na^+ channels resulting from background depolarization. Note that the threshold synaptic conductance required to trigger branch events in the face of synaptic background was identical to that required when background was absent. The five branches receiving input together drove a sustained depolarization of the tuft (two-headed arrow in the spatiotemporal plot, Fig. 8, right), and a 12 mV depolarization in the distal trunk. Background appeared to diminish the spread of firing from one branch to the next, and despite the activity in the tuft branches little effect was measured in either the soma or in mid-trunk.

(3) As input increased to 4 nS per branch, 20 nS in total, a more sustained tuft depolarization occurred, which charged up the apex of the apical trunk, causing initiation of Na^+ current-driven spikes in the distal trunk, the same sequence of events that occurred without background. Na^+ firing threshold was a few millivolts higher than that without background, presumably because the available Na^+ channel density was diminished by inactivation since resting potential in the distal dendrites was depolarized 9 mV with background on. Despite the background synaptic conductances present throughout the apical dendrite, once

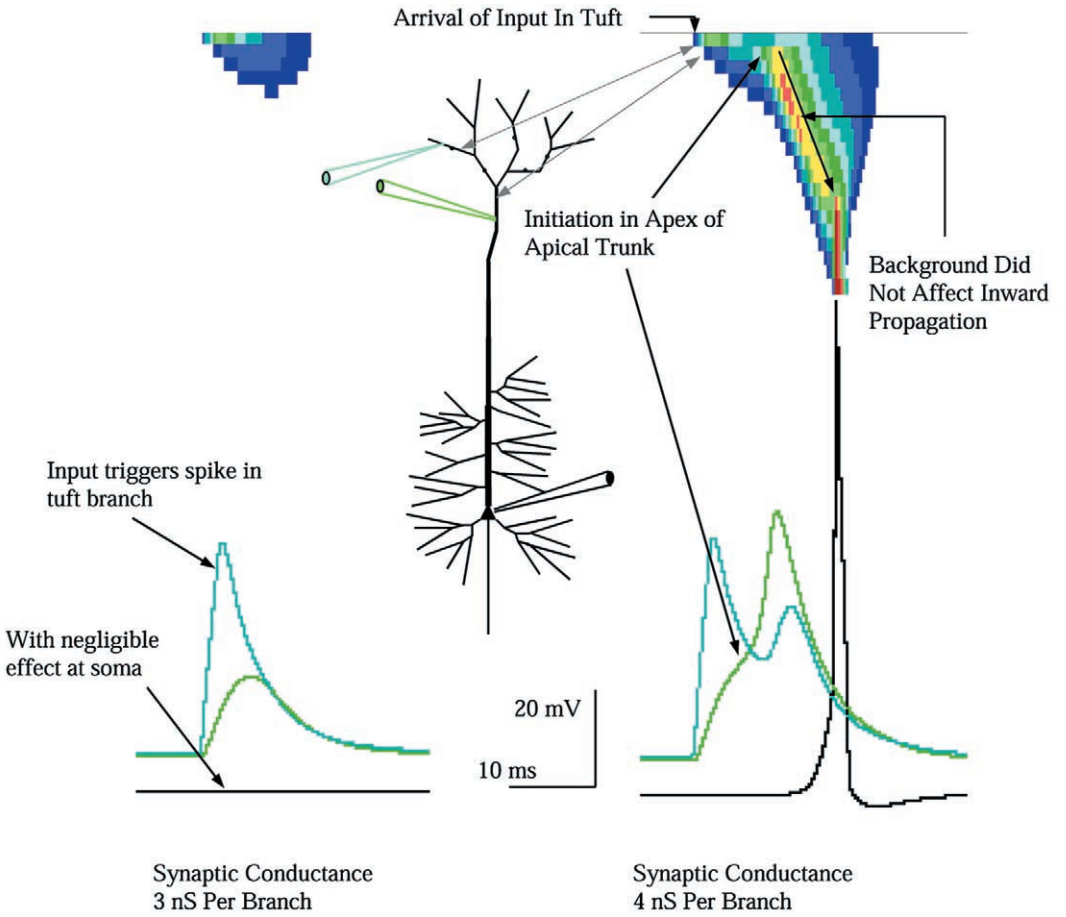

Figure 8. Uniform background did not diminish the effectiveness of tuft input

Uniform background present in both cases. Left, at 3 nS synaptic input per branch, synaptic currents activated sufficient Na^+ current to drive a regenerative spike in the branches receiving input, reaching about −22 mV (40 mV above rest). Depolarization in the tuft was more localized, with little effect on voltage in the trunk (green trace), and none at the soma. Right, when input reached about 4 nS per branch, 20 nS of tuft input in total, a more sustained tuft depolarization occurred which in turn charged the apex of the apical trunk to Na^+ firing threshold, about −41 mV. This was the critical event for initiation. Once the apex of the trunk fired, that event propagated inward along the trunk. Propagation inward was little affected by the background synaptic conductances present.

firing initiated in the distal trunk it propagated inward reliably and fired the soma when arriving there.

Proximal input in the presence of background

In contrast to the unimpaired efficacy of tuft input, the background markedly dampened the effect of proximal input to the apical oblique dendritic branches. The proximal input still readily triggered Na^+ spikes in the branches receiving input, but in the presence of background the firing of branches tended to be more isolated and did not readily spread to adjacent sub-branches. Further the spread of depolarization along the trunk was curtailed. As a result, we found it difficult to drive firing in the cell. Indeed, for input distributed to five oblique branch segments, 160 nS of input was insufficient to fire the cell (result not shown).

Since the spatial pattern of synaptic input influences its effectiveness (Rall, 1970) we explored other spatial distributions amongst the apical oblique branches, finding that when we divided input over 10 (rather than 5) recipient apical oblique sub-branches 70 nS total input triggered firing. Causing 10 branches to fire can be more effective than driving five with twice the input per branch because branch firing is all-or-none, so dividing input over more sub-branches can be more effective, provided each sub-branch still receives enough input to fire (Kuno & Llinás, 1970; Rhodes, 1999).

It should be emphasized that we utilized simple repetitive barrages of synaptic stimulus; the relative efficacy of proximal inputs to oblique branches may be favoured by more complex spatiotemporal patterns of synaptic input arrival which remain to be explored. Further, the relative efficacy of input to the basal arbor has not been probed in the present study. With those caveats, we found the conclusion that uniform background diminished the effectiveness of input to the apical oblique branches, and thereby enhanced the relative efficacy advantage of layer 1 input to the apical tuft, to be robust across variations of spatial input distributions within these two input regions.

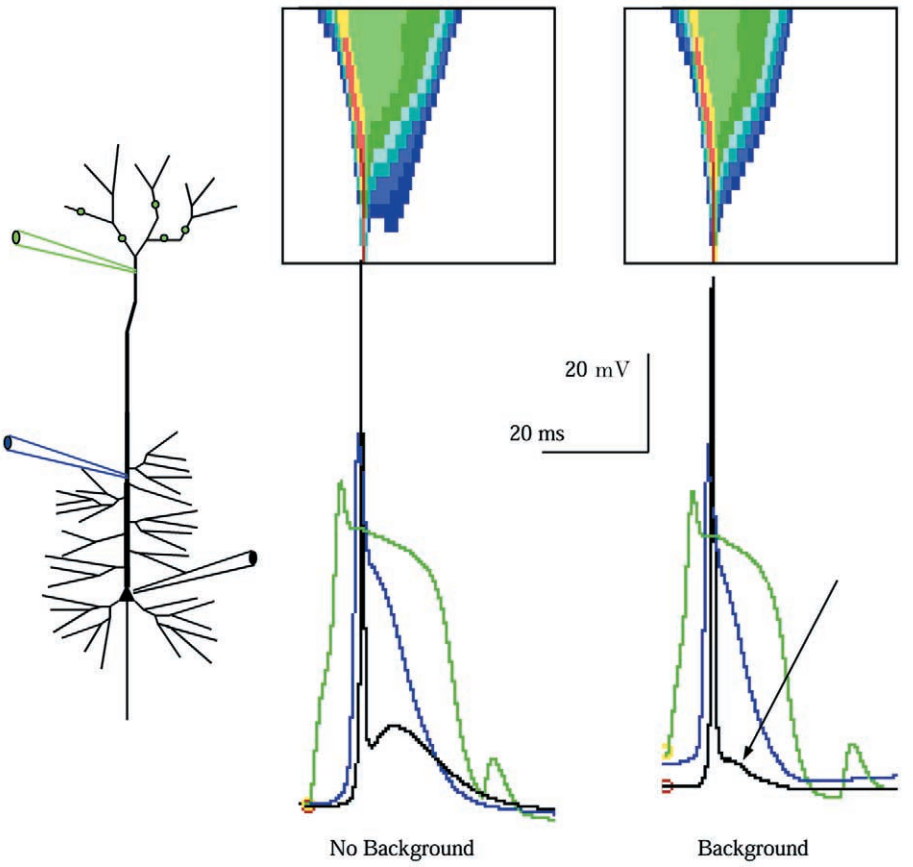

Figure 9. Background does not diminish the distal Ca^{2+} spike, but may reduce its inward drive at the soma

The distal Ca^{2+} spike triggered by tuft input is compared with (at right) and without (at left) the simulated background. The voltage axis is aligned for both records; the discrepancy in resting potential levels for both soma and dendrites arises from the net background synaptic drive. Note that while the background had little effect upon the Ca^{2+} spike's amplitude and duration in the distal apical trunk (green trace), it profoundly diminished the after-depolarizing potential driven at the soma (arrow).

The integration of synaptic inputs in an apical dendrite supporting Ca^{2+} spikes when background is present

Dendritic Ca^{2+} events have been observed in layer 5 cells in 5- to 8-week-old rats *in vivo* using two-photon [Ca^{2+}] imagery (Helmchen *et al.* 1999), but under anaesthesia, which may curtail the level of background activity. What effect might the synaptic background present during waking activity have upon the distal dendritic Ca^{2+} events observed in mature layer 5 cells? In the presence of background, is there any diminution of synaptic efficacy in response to layer 1 input to a mature apical dendrite? We found none (Fig. 9). The background utilized in these simulations (see Methods) had little effect on the initiation of the dendritic Ca^{2+} event itself, little effect on the propagation of excitation inward along the trunk to fire the soma, and as described above paradoxically enhanced the advantage enjoyed by input to the apical tuft.

We did find, however, that while initiation of the dendritic Ca^{2+} current-driven plateau in the distal apical dendrite was not impaired by background, the drive on the soma exerted by the plateau was. In particular the after-depolarizing potential (ADP) which the dendritic Ca^{2+} event drives *in vitro* was absent (Fig. 9). Comparing the dendritic Ca^{2+} event and the somatic spike and ADP in the same model cell, with and without background indicates that the background had limited effect on the Ca^{2+} spike in the dendrites, shortening its duration 15% and leaving amplitude unchanged. Yet the drive exerted by that dendritic voltage plateau upon the soma was largely quenched (Fig. 9). Thus we find that although background membrane conductance did not impair active propagation along the trunk, it did diminish the net axial ohmic flow of current from the site of the depolarizing plateau reaching the soma. Models of burst generation in layer 5 cells have held that this inward axial flow drives bursts (Rhodes & Gray, 1994), a hypothesis consistent with data from dual impalement records (Stuart *et al.* 1997; Larkum *et al.* 1999*a*,*b*). It may be, therefore, that the relationship between the Ca^{2+} spike in the distal apical dendrite and the generation of bursts in layer 5 cells is more complex *in vivo*, perhaps dependent upon transient cessation of local shunting inhibition to the trunk membrane.

DISCUSSION

We have examined the integration of excitatory synaptic inputs in the apical dendrite of simulated neocortical layer 5 pyramidal cells, both with and without the presence of synaptic background. The conclusions can be summarized as follows.

(1) It appears that synaptic input to the apical tuft of layer 5 pyramidal cells may be at least twice as effective in triggering cell firing as equal input to the proximal apical branches *in vitro*, and that this advantage is enhanced when a uniform background is applied. This general conclusion obtained irrespective of whether the dendritic tree supported the Ca^{2+} events which appear to be typical in layer 5 cells reaching maturity in their channel distribution (aged about P28 or older). The essential mechanism was not inward propagation, but rather a combination of two factors: first, the tuft seems to be prone to sustained depolarization under a variety of membrane and background assumptions; and second, there is well matched axial linkage between the nexus of the tuft and the distal trunk. Thus, following appropriate layer 1 fibre stimulation, branches in the tuft depolarize, causing a sustained tuft depolarization which charges the apex of the apical trunk towards firing threshold. Because of the smooth taper of the trunk itself, once initiated in the distal nexus (Rhodes, 1999; Larkum *et al.* 1999*a*,*b*) propagation along the trunk to the soma may proceed inward. Interestingly, at physiologically plausible trunk Na^+ channel density, inward propagation may be fragile, subject to control by hyperpolarizing currents in the trunk, modulation of trunk Na^+ channels (Rhodes, 1999), as well as by both excitatory (Larkum *et al.* 2001) and inhibitory (Llinás, 1975) inputs ahead of the path of propagation.

The total layer 1 input required to fire the cell (about 20 nS in the examples here) would correspond to perhaps 15–30 individual unitary events if conductance at individual terminals is equivalent to that estimated for corticocortical inputs to layer 4 stellate cells (Gil & Amitai, 1996).

(2) It appears that for neocortical layer 5 pyramidal cells the notion of a single integration zone where inputs are summed and initiation of firing is decided is an oversimplification. Rather, our results suggest that initiation of regenerative activity can be quite variable. It may occur at the apex of the distal trunk, at the axon, or simultaneously across a stretch of the apical trunk. Indeed, initiation can shift amongst these and perhaps other alternatives from moment to moment, even across a series of identical repeated inputs (Turner *et al.* 1991; Zecevic & Antic, 1998; Antic *et al.* 2001). Among the reasons for the shifting of the locus of initiation is that the available Na^+ channel density along the trunk shifts due to its inactivation as a function of voltage history.

Reports of the responses of layer 5 cells to proximal apical synaptic input *in vitro* have focused upon the axonal initiation which occurs with moderate proximal input (Stuart & Sakmann, 1994; Stuart *et al.* 1997) but our results suggest that the hillock is not causally relevant to the processes of integration for many spatiotemporal input histories. As has been shown in mitral cells of the olfactory bulb by Sheperd and colleagues (Chen *et al.* 1997) distal input tends to trigger initiation in the distal trunk, as had been suggested by current source density analyses of hippocampal pyramidal cells (Herreras, 1990; Turner *et al.* 1991). The central role for the axon hillock in

integration and initiation was proposed in connection with the classic motoneuron investigations of the 1950s (Eccles, 1957) and may be more applicable to that cell type, which appears to have relatively unexcitable dendritic membrane (Lüscher & Larkum, 1998).

(3) In the presence of a uniform synaptic background we found that the relative advantage of tuft over proximal input in firing the cell was enhanced. This somewhat unexpected finding arose because the background curtailed the passive spread of charge along the trunk, which reduced the effectiveness with which inputs to apical oblique branches combine. In contrast, neither the coupling between the tuft and the apex of the trunk, nor the inward propagation along the apical trunk, key factors mediating the linkage between tuft input and somatic firing, were impaired by background. The results imply that in background layer 1 input fires the cell readily, emphasizing the possible importance of this input pathway *in vivo*.

A very simple pattern of input

The study was restricted to a single spatial pattern of proximal and of distal input, with inputs arriving in a simple train of barrages. Thus the consequences of spatiotemporal structure in the patterning of input have not been explored, and our results come with this caveat. It will be of interest to determine how these results extend for stimuli organized into bursts or other temporal patterns characteristic of neuronal activity *in vivo* (Dobrunz & Stevens, 1999), particularly because the presence of voltage-gated dendritic currents ensures a non-linear relationship between input and response. Further, we have also neglected the complexities of synaptic action at each release site, including short term dynamics of release (e.g. Thomson *et al.* 1993; Wang & Stevens, 1994) as well as postsynaptic dynamic mechanisms such as receptor saturation and desensitization (Trussell & Fischback, 1989). Examining the present results in the context of physiologically meaningful patterns of input will be a subject of subsequent work.

The simulated background

The NMDA component of background conductance has not been included in prior simulations to our knowledge. This is an active component of the background, in that the voltage sensitivity of the NMDA channel causes its current to increase when local dendritic voltage increases. Even though we incorporated a fairly low NMDA background conductance per synapse (one-quarter that of the AMPA component on average), the much longer mean open time of the NMDA channel resulted in a higher average background NMDA conductance density (Table 1), so that this background current rises in dendritic branches which are depolarized, a positive feedback loop which may contribute to the importance of NMDA conductance in cortical responsiveness *in vivo*. To adequately assess the effects of the active non-linearity represented by the NMDA component of background conductance upon synaptic integration in pyramidal cell dendritic trees will require much further work.

We note that the background conductance parameters utilized in this study cannot be uniquely determined by somatic impalement measurements such as those in Destexhe & Paré (1999). However, our conclusions are not likely to depend on the details of the background, since without any background tuft input was already more effective than proximal apical input, an efficacy advantage which background enhanced.

Finally, it should be emphasized that modelling background input as uniform, with no spatial and temporal patterning, is obviously a simplification. It may be that our conclusions would be altered when re-examined in the presence of background better reflecting the spatio-temporal patterns of background input found in the cortex during the waking state, but at present little data are available to inform such an improvement.

The role of dendritic Ca^{2+} events in synaptic integration and initiation

In vitro studies suggest Ca^{2+} events are common in the distal apical dendrite of relatively mature (P28 or older) layer 5 cells (Amitai *et al.* 1993; Schiller *et al.* 1997; Stuart *et al.* 1997; Larkum *et al.* 1999*a*,*b*; Zhu, 2000). When dendritic currents producing such events were included, the simulated responses to input to both tuft and proximal apical dendrite suggested that Ca^{2+} spikes do not play a causal role in initiation, but rather are themselves triggered by and so follow a Na^+ current-driven initial regenerative event (Larkum *et al.* 1999*b*). However, once the dendritic Ca^{2+} event is produced in the apical dendrite, it may exert influence on the integration of synaptic inputs in a number of ways. It can transform the consequence of a synaptic input from a single spike to a burst by driving subsequent somatic spikes, with the vigour of the dendritic event and resultant somatic burst markedly increasing between ages P14 and P42 (Zhu, 2000). We also found preliminary indications that the inward drive of a distant dendritic Ca^{2+} event may be shunted by background. Moreover, following the sustained Ca^{2+} entry during a dendritic Ca^{2+} spike in our simulations $[Ca^{2+}]$-gated K^+ currents rendered the dendritic tree damped to subsequent input while $[Ca^{2+}]$ levels recovered. Assessment of whether these effects are in fact important aspects of the integration of synaptic inputs in dendritic trees which produce Ca^{2+} spikes will benefit from more data on the densities and properties of dendritic $[Ca^{2+}]$-gated K^+ currents, about which very little is currently known.

The effects of distal dendritic I_h

In addition to the increase in dendritic Ca^{2+} current, with maturation layer 5 cells also display a high distal density of the hyperpolarization-activated current (I_h), with its distribution appearing to increase with distance from the

soma (Williams & Stuart, 2000; Berger *et al.* 2001) as has been observed in hippocampal CA1 pyramidal cells (Magee, 1998). Among the consequences is that input resistance in the tuft is dramatically reduced (Zhu, 2000). We briefly examined the implications for tuft input integration by adding dendritic I_h with kinetics and density distribution suggested by these recent reports, and found that the present results on tuft input efficacy did not change (authors' unpublished results).

Two aspects of this observation were somewhat counterintuitive: first, even after the addition of distal I_h and a $>300\,\%$ reduction in R_{in} in the distal trunk and primary tuft branches (as seen by Zhu, 2000), the tertiary tuft branches which receive most of the inputs remained of high impedance (>250 MΩ). As a result, synaptic inputs to the tertiary tuft branches still readily drive voltage above regenerative threshold for both Na^+ and Ca^{2+} currents. Second, despite the shorter time constant implied by the low R_{in}, tuft electrotonic geometry continued to favour a sustained depolarization, just as was the case when the apparent membrane time constant was greatly reduced by the presence of simulated background (cf. Fig. 8). Thus the sustained depolarization exhibited by the tuft is not dependent upon the passive properties of the membrane.

Modulation of inward propagation along the apical trunk

Our results suggest that the propensity of apical tuft input to fire the cell depends upon the inward propagation of a regenerative Na^+ current-driven spike initiated at the apex of the distal trunk. There exist hyperpolarizing K^+ currents in the membrane of the apical trunk, which can curtail inward propagation along the trunk and therefore control the effect of tuft input, which were either excluded from our study or included only at low densities. Those most suited to interfere with fast Na^+ channel-dependent propagation are probably currents which can activate rapidly, and which activate at or near rest, including the families of currents known as A-currents and M-currents (Storm, 1990). Further, the apical trunk Na^+ channel density we incorporated was inferred from reported measurements of backpropagation *in vitro* (Stuart *et al.* 1997; Larkum *et al.* 1999*a*,*b*), and the assumption that a similar Na^+ conductance properties exist *in vivo* remains to be justified experimentally.

Finally, modulators which either upregulate K^+ currents along the trunk, or which downregulate Na^+ channels there (Rhodes, 1997, 1999) could effectively curtail the efficacy of layer 1 input by blocking inward propagation. Alternatively, downregulation of these K^+ currents, for example the effect of ACh on I_M or the reduction of A-current activation caused by noradrenalin via protein kinase A (Hoffman & Johnston, 1998), may facilitate the ease with which tuft input fires the cell (Rhodes, 1998). The sensitivity of distal initiation and inward propagation along the trunk to these and other modulators provides a mechanism for the state-dependent control of the linkage between tuft input and somatic firing, a subject we believe warrants much further examination, both in simulations and in experiment when feasible.

Inputs to layer 5 cells should be assessed in the context of the cortical circuit in which they are embedded

We have examined the responses of a layer 5 cell as if it were isolated from the circuitry in which it is embedded. For example, it is likely that the layer 1 inputs reaching a layer 5 cell also terminate upon adjacent layer 2/3 pyramidal cell tufts. In this regard, it is significant that Thomson & Bannister (1998) report strong vertical connectivity from layer 2/3 to layer 5 cells within a ~100 μm diameter cylinder (a 'microcolumn'). Further, they find these synaptic connections are 10-fold more likely to terminate upon layer 5 cells of the morphological type we have modelled, which tend to be bursting (Larkman & Mason, 1990; Chagnac-Amitai *et al.* 1990), than onto regular spiking layer 5 cells, which lack an elaborate layer 1 tuft. There thus appears to be a vertical relay within a microcolumn allowing layer 1 input to establish an active microcolumn, in which layer 2/3 along with layer 5 bursting cells fire.

Layer 1 input also impinges upon the dendrites of interneurons. Two recently reported aspects of the anatomy of this projection should be noted here. First, in contrast to the strong monosynaptic feedforward inhibition in most corticocortical projections (Douglas *et al.* 1991), layer 1 input fibres conveying higher-to-lower area cortical projections (corticocortical backprojections) have been reported to impinge mainly on the distal portions of parvalbumin-positive local interneurons, and with smaller synaptic terminations than those found in the reciprocal forward projection (Gonchar & Burkhalter, 1999*a*). Thus layer 1 inputs may be comparatively ineffective in eliciting feedforward inhibition via parvalbumin-positive fast spiking interneurons (see also Shao & Burkhalter, 1999). Second, the layer 1 fibres conveying cortical backprojections have been recently noted to impinge upon calretinin-positive interneurons which in turn inhibit a local system of interneurons (Gonchar & Burkhalter, 1999*b*). This disynaptic disinhibition could facilitate excitation of cells in the target area.

Collecting the observations noted above, it seems that layer 1 input sets up activity of layer 2/3 and tufted layer 5 cells in register, elicits limited feedforward inhibition upon its target pyramidal cells, and disinhibits its targets by exciting a set of interneurons which themselves target nearby interneurons. We begin to suspect that the special responsiveness of layer 5 cells to layer 1 input may be just one component of a coordinated suite of circuit relationships which have evolved together to ensure that layer 1 input, the primary route for cortiocortical backprojections (Rockland & Pandya, 1979;

Rockland & Virga, 1989; Cauller & Connors, 1992, 1994) and thalamic intralaminar input (Cunningham & LeVay, 1986) can readily activate a vertically interconnected microcolumn.

In conclusion, we have found that apical tuft input is specially suited to cause layer 5 cell firing, and surprisingly that its paradoxical advantage over more proximal input is enhanced by the presence of uniform synaptic background adequate to reproduce the 4- to 5-fold drop in R_{in} recently reported to *in vivo* (Destexhe & Paré, 1999). It is intriguing that the layer 1 fibre system is a very primitive feature of cortex, found in three-layer turtle dorsal cortex and piriform cortex, as well as the more recently evolved six-layer neocortex, and that the apical tuft of pyramidal cells and its precise spatial correspondence with layer 1 are evolutionarily ancient features (Ramon y Cajal, 1911, cf. Fig. 545). One is led to conjecture that there is a fundamental aspect of cortical functioning which is associated with the ability of layer 1 input to fire pyramidal cells. It has been suggested, for example, that the input from higher to lower cortical areas triggers associative recall and imagery (Rhodes, 1990). If borne out by experiment, our simulation results suggest that the layer 1 fibre system, which is so primitive phylogenetically, may be of heretofore unforeseen importance in cortical function.

Amitai, Y., Friedman, A., Connors, B. W. & Gutnick, M. J. (1993). Regenerative electrical activity in apical dendrites of pyramidal cells in neocortex. *Cerebral Cortex* **3**, 26–38.

Andreason, M. & Lambert, J. D. C. (1995). Regenerative properties of pyramidal cell dendrites in area CA1 of the rat hippocampus. *Journal of Physiology* **483**, 421–441.

Antic, S., Wuskell, J. P., Loew, L. & Zecevic, D. (2001). Functional profile of the giant metacerebral neuron of *Helix aspersa*: temporal and spatial dynamics of electrical activity *in situ*. *Journal of Physiology* **527**, 55–69.

Bekkers, J. M. (2000*a*). Properties of voltage-gated potassium currents in nucleated patches from large layer 5 cortical pyramidal neurons of the rat. *Journal of Physiology* **525**, 593–609.

Bekkers, J. M. (2000*b*). Distribution and activation of voltage-gated potassium channels in cell-attached and outside-out patches from large layer 5 cortical pyramidal neurons of the rat. *Journal of Physiology* **525**, 611–620.

Berger, T., Larkum, M. E. & Lüscher, H.-R. (2001). High I_h channel density in the distal apical dendrite of layer V pyramidal cells increases bidirectional attenuation of EPSPs. *Journal of Neurophysiology* **83**, 855–868.

Bernander, O., Douglas, R. J., Martin, K. A. & Koch, C. (1991). Synaptic background activity influences spatiotemporal integration in single pyramidal cells. *Proceedings of the National Academy of Sciences of the USA* **88**, 11569–11573.

Cauller, L. J. & Connors, B. W. (1992). Functions of very distal dendrites: experimental and computational studies of layer I synapses on neocortical pyramidal cells. In *Single Neuron Computation*, ed. McKenna, T., Davis, J. & Zornetzer, S. F., pp. 199–230. Academic Press, San Diego.

Cauller, L. J. & Connors, B. W. (1994). Synaptic physiology of horizontal afferents to layer I in slices of rat S1 neocortex. *Journal of Neuroscience* **14**, 751–762.

Chagnac-Amitai, Y., Luhmann, H. J. & Prince, D. A. (1990). Burst generating and regular spiking layer 5 pyramidal neurons of rat neocortex have different morphological features. *Journal of Comparative Neurology* **296**, 598–613.

Chen, W. R., Midtgaard, J. & Shepherd, G. M. (1997). Forward and backward propagation of dendritic inpulses and their synaptic control in mitral cells. *Science* **278**, 463–467.

Colbert, C. M. & Johnston, D. (1996). Axonal action-potential initiation and Na^+ channel densities in the soma and axon initial segment of subicular pyramidal neurons. *Journal of Neuroscience* **16**, 6676–6686.

Cunningham, E. T. & Levay, S. (1986). Laminar and synaptic organization of the projection from the thalamic nucleus centralis to primary visual cortex in the cat. *Journal of Comparative Neurology* **254**, 65–77.

Desan, P. H. (1994). The organization of the cerebral cortex of the pond turtle *Pseudemys scripta elegans*. PhD Thesis, Harvard University.

Destexhe, A. & Paré, D. (1999). Impact of network activity on the integrative properties of neocortical pyramidal neurons in vivo. *Journal of Neurophysiology* **81**, 1531–1547.

Dobrunz, L. E. & Stevens, C. F. (1999). Response of hippocampal synapses to natural stimulation patterns. *Neuron* **22**, 157–166.

Douglas, R. J., Martin, K. A. & Whitteridge, D. (1991). An intracellular analysis of the visual responses of neurones in cat visual cortex. *Journal of Physiology* **440**, 659–696.

Eccles, J. C. (1957). *The Physiology of Nerve Cells*. Johns Hopkins Press, Baltimore.

Gil, Z. & Amitai, Y. (1996). Properties of convergent thalamocortical and intracortical synaptic potentials in single neurons of neocortex. *Journal of Neuroscience* **16**, 6567–6578.

Gonchar, A. & Burkhalter, A. (1999*a*). Differential subcellular localization of forward and feedback interareal inputs to parvalbumin expressing GABAergic neruons in rat visual cortex. *Journal of Comparative Neurology* **406**, 346–360.

Gonchar, A. & Burkhalter, A. (1999*b*). Connectivity of GABAergic caltetinin-immunoreactive neurons in rat primary visual cortex. *Cerebral Cortex* **9**, 683–696.

Hamill, O. P., Hugenard, J. R. & Prince, D. A. (1991). Patch-clamp studies of voltage-gated currents in identified neurons of the rat cerebral cortex. *Cerebral Cortex* **1**, 48–61.

Helmchen, F., Imoto, K. & Sakmann, B. (1996). Ca^{2+} buffering and action potential-evoked Ca^{2+} signalling in dendrites of pyramidal neurons. *Biophysical Journal* **70**, 1069–1081.

Helmchen, F., Svoboda, K., Denk, W. & Tank, D. W. (1999). *In vivo* dendritic calcium dynamics in deep-layer cortical pyramidal neurons. *Nature Neuroscience* **2**, 989–996.

Herreras, O. (1990). Propagating dendritic action potential mediates synaptic transmission in CA1 pyramidal cells in situ. *Journal of Neurophysiology* **64**, 1429–1441.

Hoffman, D. A. & Johnston, D. (1998). Downregulation of transient K^+ channels in dendrites of hippocampal CA1 pyramidal neurons by activation of PKA and PKC. *Journal of Neuroscience* **18**, 3521–3528.

Holmes, W. R. & Woody, C. D. (1989). Effects of uniform and non-uniform synaptic "activation-distributions" on the cable properties of modeled cortical pyramidal neurons. *Brain Research* **505**, 12–22.

Huguenard, J. R., Hamill, O. P. & Prince, D. A. (1989). Sodium channels in dendrites of rat cortical pyramidal neurons. *Proceedings of the National Academy of Sciences of the USA* **86**, 2473–2477.

Johnston, D., Magee, J. C., Colbert, C. M. & Christie, B. R. (1996). Active properties of neuronal dendrites. *Annual Review of Neuroscience* **19**, 165–186.

Kamondi, A., Acsdy, L. & Buzski, G. (1998). Dendritic spikes are enhanced by cooperative network activity in the intact hippocampus. *Journal of Neuroscience* **18**, 3919–3928.

Kim, H. G. & Connors, B. W. (1993). Apical dendrites of the neocortex: correlation between sodium- and calcium-dependent spiking and pyramidal cell morphology. *Journal of Neuroscience* **13**, 5301–5311.

Kuno, M. & Llinás, R. (1970). Alterations of synaptic action in chromatolysed motoneurones of the cat. *Journal of Physiology* **210**, 823–838.

Larkman, A. U. (1991). Dendritic morphology of pyramidal neurones of the visual cortex of the rat: III. Spine distributions. *Journal of Comparative Neurology* **306**, 332–343.

Larkman, A. U. & Mason, A. J. R. (1990). Correlations between morphology and electrophysiology of pyramidal neurones in slices of rat visual cortex. I. Establishment of cell classes. *Journal of Neuroscience* **10**, 1407–1414.

Larkum, M. E., Kaiser, K. M. M. & Sakmann, B. (1999*a*). Calcium electrogenesis in distal apical dendrites of layer 5 pyramidal cells at a critical frequency of back-propagating action potentials. *Proceedings of the National Academy of Sciences of the USA* **96**, 14600–14604.

Larkum, M. E., Zhu, J. J. & Sakmann, B. (1999*b*). A new cellular mechanism for coupling inputs arriving at different cortical layers. *Nature* **398**, 338–341.

Larkum, M. E., Zhu, J. J. & Sakmann, B. (2001). Dendritic mechanisms underlying the coupling of the dendritic with the axonal action potential initiation zone of adult rat layer 5 pyramidal neurones. *Journal of Physiology* **533**, 447–466.

Llinás, R. (1975). Electroresponsive properties of dendrites in central neurons. *Advances in Neurology* **12**, 1–13.

Llinás, R. (1988). The intrinsic electrophysiological properties of mammalian neurons: insights into central nervous system function. *Science* **242**, 1654–1664.

Llinás, R., Nicholson, C., Freeman, J. A. & Hillman, D. E. (1968). Dendritic spikes and their inihibition in alligator Purkinje cells. *Science* **160**, 1133–1135.

Lüscher, H. R. & Larkum, M. E. (1998). Modeling action potential initiation and back-propagation in dendrites of cultured rat motoneurons. *Journal of Neurophysiology* **80**, 715–729.

McCormick, D. A., Connors, B. W., Lighthall, J. W. & Prince, D. A. (1985). Comparative electrophysiology of pyramidal and sparsely spiny stellate neurons of the neocortex. *Journal of Neurophysiology* **54**, 782–806.

Magee, J. (1998). Dendritic hyperpolarization-activated currents modify the integrative properties of hippocampal CA1 pyramidal neurons. *Journal of Neuroscience* **18**, 7613–7624.

Mainen, Z. F., Joerges, J., Huguenard, J. R. & Sejnowski, T. J. (1995). A model of spike initiation in neocortical pyramidal neurons. *Neuron* **15**, 1427–1439.

Mason, A. J. R. & Larkman, A. U. (1990). Corelations between morphology and electrophysiology of pyramidal neurons in slices of rat visual cortex. *Journal of Neuroscience* **10**, 1415–1428.

Mel, B. W. (1994). Information processing in dendritic trees. *Neural Computation* **6**, 1031–1085.

Rall, W. (1964). Theoretical significance of dendritic trees for neuronal input-output relations. In *Neural Theory and Modeling*, ed. Reiss, R. F., pp. 73–97. Stanford University Press, Palo Alto.

Rall, W. (1970). Cable properties of dendrites and effects of synaptic location. In *Excitatory Synaptic Mechanisms*, ed. Andersen, P. & Jansen, J. K. S. Jr. Universitatsforlag, Oslo.

Ramon y Cajal, S. (1911). *Histologie du Système Nerveux de l'Homme et des Vertebrates*. Maloine, Paris.

Rhodes, P. A. (1990). A computational study indicates cross-modal association arises naturally in the neocortex via feedback projections. *Society for Neuroscience Abstracts* **16**, 286.

Rhodes, P. A. (1997). Neuronal functional properties are very sensitive to shifts in the voltage dependence of Na^+ channel inactivation. *Society for Neuroscience Abstracts* **23**, 653.

Rhodes, P. A. (1998). Modulation of the dendritic Kv4.2 channels regulates synaptic integration and backpropagation in pyramidal cell dendrites. *Annals of the New York Academy of Sciences* **868**.

Rhodes, P. A. (1999). Functional implications of active currents in the dendrites of pyramidal neurons. In *Cerebral Cortex*, vol. 13, ed. Ulinski, P., Jones, E. G. & Peters, A., pp. 139–200. Plenum Press, New York.

Rhodes, P. A. & Gray, C. M. (1993). Effects of electrically active dendrites and NMDA-type synaptic conductances. *Society for Neuroscience Abstracts* **19**, 242.

Rhodes, P. A. & Gray, C. M. (1994). Simulations of intrinsically bursting neocortical pyramidal neurons. *Neural Computation* **6**, 1086–1110.

Rhodes, P. A. & Llinás, R. (1999). Pyramidal cells *in vivo* may be most sensitive to synaptic input to the apical tuft. *Society for Neuroscience Abstracts* **25**, 1739.

Rhodes, P. A., Yuste, R. & Tank, D. W. (1995). Ca^{2+} and Na^+ channels throughout the basal dendrites of regular spiking neocortical pyramidal neurons: implications of bursting with EGTA. *Society for Neuroscience Abstracts* **21**, 1996.

Richardson, T. L., Turner, R. W. & Miller, J. J. (1987). Action potential discharge in hippocampal CA1 pyramidal neurons: current source-density analysis. *Journal of Neurophysiology* **58**, 981–996.

Rockland, K. S. & Pandya, D. (1979). Laminar origins and terminations of cortical connections of the occipital lobe in rhesus monkey. *Brain Research* **179**, 3–20.

Rockland, K. S. & Virga, A. (1989). Terminal arbors of individual "feedback" axons projecting from area V2 to V1 in the macaque monkey: a study using immunohistochemistry of anterogradely transported *Phaseolus vulgaris*-leucoagglutinin. *Journal of Comparative Neurology* **285**, 54–72.

Schiller, J., Helmchen, F. & Sakmann, B. (1995). Spatial profile of dendritic calcium transients evoked by action potentials in rat neocortical pyramidal neurones. *Journal of Physiology* **487**, 583–600.

Schiller, J., Schiller, Y., Stuart, G. & Sakmann, B. (1997). Calcium action potentials restricted to distal apical dendrites of rat neocortical pyramidal neurons. *Journal of Physiology* **505**, 605—616.

Schwindt, P. C., Spain, W. J., Fochring, R. C., Stafstrom, C. E., Chubb, M. C. & Crill, W. E. (1988). Multiple potassium conductances and their functions in neurons from cat sensorimotor cortex in vitro. *Journal of Neurophysiology* **59**, 424–449.

Seamans, J. K., Gorelova, N. A. & Yang, C. R. (1997). Contributions of voltage-gated Ca^{2+} channels in the proximal versus distal dendrites to synaptic integration in prefrontal cortical neurons. *Journal of Neuroscience* **15**, 5936–5945.

Shao, Z. & Burkhalter, A. (1999). Role of $GABA_B$ receptor-mediated inhibition in reciprocal interareal pathways of rat visual cortex. *Journal of Neurophysiology* **81**, 1014–1024.

Spencer, W. A. & Kandel E. R. (1961). Electrophysiology of hippocampal neurons. IV. Fast prepotentials. *Journal of Neurophysiology* **24**, 272–285.

Storm, J. F. (1990). Potassium currents in hippocampal pyramidal cells. *Progress in Brain Research* **83**, 161–187.

Stratford, K. J., Mason, A. J. R., Larkman, A. U., Major, G. M. & Jack, J. J. B. (1989). The modeling of pyramidal neurones in the visual cortex. In *The Computing Neuron*, ed. Durbin, R. M., Miall, R. C. & Mitchison, G. J., pp. 296–321. Addison-Wesley, Wokingham, UK.

Stuart, G. J. & Sakmann, B. (1994). Active propagation of somatic action potentials into neocortical pyramidal cell dendrites. *Nature* **367**, 69–72.

Stuart, G., Schiller, J. & Sakmann, B. (1997). Action potential initiation and propagation in rat neocortical pyramidal neurons. *Journal of Physiology* **505**, 617–632.

Thomson, A. M. & Bannister, A. P. (1998). Postsynaptic pyramidal target selection by descending layer III pyramidal axons: dual intracellular recordings and biocytin filling in slices of rat neocortex. *Neuroscience* **84**, 669–683.

Thomson, A. M., Deuchars, J. & West, D. C. (1993). Large, deep layer pyramid-pyramid single axon EPSP's in slices of rat motor cortex display paired pulse and frequency-dependent depression, mediated presynaptically and self-facilitation, mediated postsynaptically. *Journal of Neurophysiology* **70**, 2354–2369.

Trussell, L. O. & Fischback, G. D. (1989). Glutamate receptor desensitization and its role in synaptic transmission. *Neuron* **3**, 209–218.

Turner, R. W., Meyers, D. E., Richardson, T. L. & Barker, J. L. (1991). The site for initiation of action potential discharge over the somatodendritic axis of rat hippocampal CA1 pyramidal neurons. *Journal of Neuroscience* **11**, 2270–2280.

Ulinski, P. (1990). The cerebral cortex of reptiles. In *Cerebral Cortex* vol. 8A, ed. Jones, F. G. & Peters, A., pp. 139–215. Plenum Press, New York.

Vogt, B. A. (1991). The role of layer 1 in cortical function. In *Cerebral Cortex*, vol. 9, ed. Peters, A. & Jones, E. G., pp. 49–80. Plenum Press, New York.

Wang, Y.-Y. & Stevens, C. F. (1994). Changes in reliability of synaptic function as a mechanism for plasticity. *Nature* **371**, 704–704.

Williams, S. R. & Stuart, G. J. (2000). Site independence of EPSP time course is mediated by dendritic I_h in neocortical pyramidal neurons. *Journal of Neurophysiology* **83**, 3177–3182.

Yuste, R., Gutnick, M. J., Saar, D., Delaney, K. D. & Tank, D. W. (1994). Calcium accumulations in dendrites from neocortical neurons: an apical band and evidence for functional compartments. *Neuron* **13**, 23–43.

Zecevic, D. & Antic, S. (1998). Fast optical measurement of membrane potential changes at multiple sites on an individual nerve cell. *Histochemical Journal* **30**, 197–216.

Zhu, J. J. (2000). Maturation of layer 5 neocortical pyramidal neurons: amplifying salient layer 1 and layer 4 inputs by Ca^{2+} action potentials in adult rat tuft dendrites. *Journal of Physiology* **526**, 571–587.

Zhu, J. J. & Connors, B. W. (1999). Intrinsic firing patterns and whisker-evoked synaptic responses of neurons in the rat barrel cortex. *Journal of Neurophysiology* **81**, 1171–1183.

Corresponding author's present address

P. A. Rhodes: 500 Australian Avenue South, Suite 110, West Palm Beach, FL 33401, USA.

Email: rhodesp@mindspring.com